VPI-E-71-10
June 1971

An Experimental and Analytical Investigation of the Ductile Fracture of Polymers

H. F. Brinson, H. Gonzalez, C. W. Stormont
Department of Engineering Mechanics

This Research was supported by the National Aeronautics and Space Administration, Grant Number NGR-47-004-051 with NASA-Ames, Moffett Field, California.

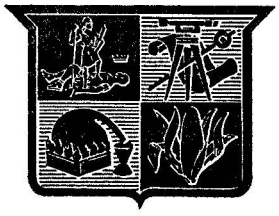

College of Engineering,
Virginia Polytechnic Institute
and State University

VPI-E-71-10
June 1971

An Experimental and Analytical Investigation of the Ductile Fracture of Polymers

H. F. Brinson, H. Gonzalez, C. W. Stormont
Department of Engineering Mechanics

This Research was supported by the National Aeronautics and Space Administration, Grant Number NGR-47-004-051 with NASA-Ames, Moffett Field, California.

College of Engineering,
Virginia Polytechnic Institute
and State University

AN EXPERIMENTAL AND ANALYTICAL INVESTIGATION OF THE DUCTILE FRACTURE OF POLYMERS

H. F. Brinson*,

H. Gonzalez**

and

C. W. Stormont***

Department of Engineering Mechanics
College of Engineering
Virginia Polytechnic Institute
and State University
Blacksburg, Virginia 24061

---

* Associate Professor

** Former graduate student now at Tennessee Eastman Company, Kingsport, Tenn.

*** Graduate Student

ABSTRACT

This paper represents an analytical and experimental investigation of the ductile fracture of polymers. The analytical portion represents an adaptation of the Dugdale model to include the effect of a uniform shear stress at the elastic-plastic interface. The solution is formulated using a complex variable approach. The effect of assuming the existence of a uniform shear stress along the plastic zone boundary is to introduce a weak logarithmic singularity at the tip of the plastic zone. The solution demonstrates the admissibility of stress states along the elastic-plastic boundary other than that normally assumed for the Dugdale model. The results of the modified problem are compared to Dugdale's predictions.

The experimental aspect represents an evaluation of an earlier investigation extending the Dugdale mathematical model to include material anisotropy. Experiments were conducted on orthotropic sheets of polycarbonate in which the desired preorientation was produced by a rolling process. Crack opening displacements were measured as a means of qualitatively verifying the theory. Crack extension was observed to deviate from the original crack line depending on initial crack orientation with respect to material orthotropy.

ACKNOWLEDGMENTS

The authors gratefully acknowledge the financial and laboratory support supplied under NASA Contract No. NGR 47-004-051. Appreciation is also extended to their colleagues at Virginia Polytechnic Institute and State University for their helpful criticisms and suggestions.

TABLE OF CONTENTS

LIST OF ILLUSTRATIONS

LIST OF SYMBOLS

a	$s + \ell$
E	Young's modulus for isotropic material
E_x, E_y	Young's modulus in x,y direction
G_{xy}	shear modulus in xy plane
i	imaginary number, $\sqrt{-1}$
ℓ	half crack length
P	external load
s	plastic zone length
T	uniform shear stress
u, v	displacements in x,y direction
x, y	cartesian coordinates
Y	constant having units of stress
z	complex variable, $x + iy$
α_i, β_i	parameters reflecting anisotropy
κ	$\frac{3 - \nu}{1 + \nu}$ (for plane stress)
ρ, θ	radial, angular coordinate in conformal plane
θ_2	arc cos $\frac{\ell}{a}$
μ	elastic shear modulus
ζ	transformed complex variable
ν	isotropic Poisson's ratio
ν_x, ν_y	Poisson's ratio in x,y direction
σ_x, σ_y	normal stress components in x,y direction
σ_ρ, σ_θ	normal stress components in ρ, θ direction in conformal plane

σ_2	$e^{i\theta_2}$
$\tau_{\rho\theta}$	shear stress in conformal plane
ϕ, ψ	Kolosov stress functions
ϕ', ψ'	denotes differentiation with respect to ζ
$\overline{\phi}$, $\overline{\psi}$	denotes complex conjugate
ω	complex transformation function

Other symbols used are defined in the body of the text.

PREFACE

This report deals with three seemingly unrelated investigations into the behavior of polymers. These areas can be identified as:

1. The adaptation of the Dugdale model to include shear stresses at the elastic-plastic interface.
2. An experimental evaluation of the extension of the Dugdale model to include material anisotropy.
3. A new interpretation of the inelastic birefringence of polycarbonate.

The first topic is discussed in Chapters 2 and 4 and the second topic is discussed in Chapters 3 and 4. These two topics represent selected portions of the Ph.D. research of the two junior authors of this report. The third topic is presented in appendix A and represents a separate investigation by the senior author of this report which was conducted during a 12 week stay at NASA-Ames during the summer of 1969.

Even though these three areas may seem unrelated, there is a unique and unifying thread. As the title of this report suggests the entire effort is related to an attempt to obtain a better understanding of fracture mechanics as related to ductile polymers. We, of course, also feel that this work will give considerable insight into the ductile fracture of metals as well.

As is well known, the Dugdale model presupposes a plastic zone to exist in front of a crack. Normally this plastic zone is assumed to be a thin extension of the crack line. However, a number of investigators have experimentally shown that the plastic zone has a width which closely approximates the thickness of the plate being tested. In

polycarbonate as well as some other materials the shape of the plastic zone resembles a candle-flame and appears to begin adjacent to, but not at, the crack tip and proceeds initially in a direction other than the crack line. Also a number of researchers have reported on and discussed the fact that different materials have variously shaped plastic zones in front of the crack tip. The first two topics itemized above represent an effort to develop mathematical models which will predict the size, shape, and direction of plastic zone growth in front of cracks using the Dugdale model as a point of departure.

In attempting to answer questions regarding the size and initial shape of plastic zones in various materials, it is felt that possible influences are the properties of the material and the stress state near a crack tip. If the cause were the latter, then admissible stress states might exist other than the stress state normally assumed for the Dugdale model (a tensile yield stress normal to the crack line on the elastic-plastic interface). Thus a uniform shear stress was assumed to exist on the elastic-plastic boundary as well as the tensile yield stress of the material. It was felt that this modification of the stress and displacement field might give rise to a plastic zone that differs from that predicted by the normal Dugdale model.

The other approach which has been used herein assumed that various shaped plastic zones occur due to the properties of the material, i.e., local anisotropy. Thus the Dugdale model was adapted to include material anisotropy and a portion of the present effort was directed toward experimentally verifying the anisotropic Dugdale model. The ultimate objective with this approach was to predict plastic zone size and shape from a knowledge of the local anisotropy of a material-polymer or metal.

The third investigation which is reported in appendix A is an attempt to obtain an understanding of the meaning of isochromatic fringes in yielded regions. As is well known, photoelasticity is one experimental technique which can be used to measure the stress fields in front of cracks. A valuable extension of the photoelastic technique would be to develop photoplasticity to an extent that would allow the experimental evaluation of stress fields inside the plastic zones which occur in front of cracks. The third endeavor is a first step in this direction.

Portions of this report have been presented at semi-annual meetings of the Society for Experimental Stress Analysis, i.e., the anisotropic study and the photoplasticity study. The latter has been accepted for publication and will shortly appear in Experimental Mechanics.

CHAPTER I

INTRODUCTION AND REVIEW

1.1 General

It is generally assumed that fracture initiation in solids is caused by some imperfection or flaw, such as a microcrack, which causes a locally high elevation of stress upon the application of a load. The complete study of the fracture process for a particular solid requires the simultaneous consideration of both the macroscopic effects such as environmental and loading conditions, the nature and composition of the material, and the microscopic phenomena occurring at the site where the fracture initiates and grows. At one end of these two diverse viewpoints, the fracture process involves the rupturing of atomic bonds. In this range, one is interested in phenomena taking place in the material within a region of diameter on the order of 10^{-7} cm. or less and molecular theories provide the avenue of approach to the problem. On the opposite end of the scale, involving material response within a region of diameter on the order of 10^{-2} cm. and greater, the tools of continuum mechanics may be used to study the phenomenon of fracture. A model to describe atomic behavior is beset by severe mathematical difficulties, and these difficulties are commonly avoided by resorting to continuum mechanics. This is a generally accepted way to integrate the complexities of the microstructure of real materials in situations where such complexities are not believed to be essential to the question under

consideration [1]*.

Since fracture initiation involves the formation of cracks from imperfections, the microstructure of the material and the loading conditions appear essential in studying the process. Various theories dealing with crack initiation and growth have been discussed by a number of investigators for crystalline materials [2] and for amorphous polymers [3]. The principal emphasis of these microstructural theories is on understanding the mechanism of fracture initiation and they tend to be primarily qualitative in nature.

On the other hand, the macroscopic theories of fracture assume the existence of microcracks or other flaws which may readily act as fracture nuclei. The size of such imperfections is assumed to be sufficiently large compared to the characteristic dimensions of the microstructure to warrant the use of a continuum mechanics viewpoint. This latter approach will be adopted throughout this investigation.

The fracture of solids will be considered as the formation of new surfaces in the material in a thermodynamically irreversible manner. The essential aspect of the phenomenon is the rupture of cohesive bonds of the medium. In simplified terms, fracture is a process involving the nucleation and growth of imperfections such as voids or cracks.

Material response under time-independent, isothermal conditions can be generally classified as ductile or brittle; however, many materials can be made to undergo a transition from the ductile state to the brittle state or vice versa. It is known that the same material

---

* Numbers is brackets [ ] refer to bibliography.

may behave in a brittle or ductile fashion depending on such factors as rate of loading, temperature, pressure, etc. [4]. From the macroscopic or continuum standpoint, the fracture of solids can be generally classified into these same two broad categories of brittle and ductile even though the details may vary with the material, the type of external loading, and the environmental conditions. Brittle fracture is a low energy failure and, for unstable loading conditions, takes place in a catastrophic manner, meaning that the fracture velocities are usually high [5]. Ductile fracture on the other hand is usually associated with large deformations, high rates of energy dissipation, and slow fracture velocities. A study of this second aspect, namely ductile fracture, is the primary concern of this investigation.

1.2 Literature Review

The importance of the localized concentration of stress in the neighborhood of sharp notches was emphasized by Inglis [6]. He found that the stress near the tip of a notch or flaw can be much greater than the remotely applied stress. As a model Inglis used the two dimensional configuration of an elliptical hole in a plate under an applied tensile stress P as depicted in Fig. 1. Inglis obtained an exact solution for this problem and his expression for the maximum stress at the apex of the major axis of the ellipse is given by

$$(\sigma_y)_{max} = P[1 + (2a/b)] \qquad (1.2.1)$$

where 2a and 2b are the major and minor diameters of the elliptical hole. In addition he showed that if the flaw is in the shape of a

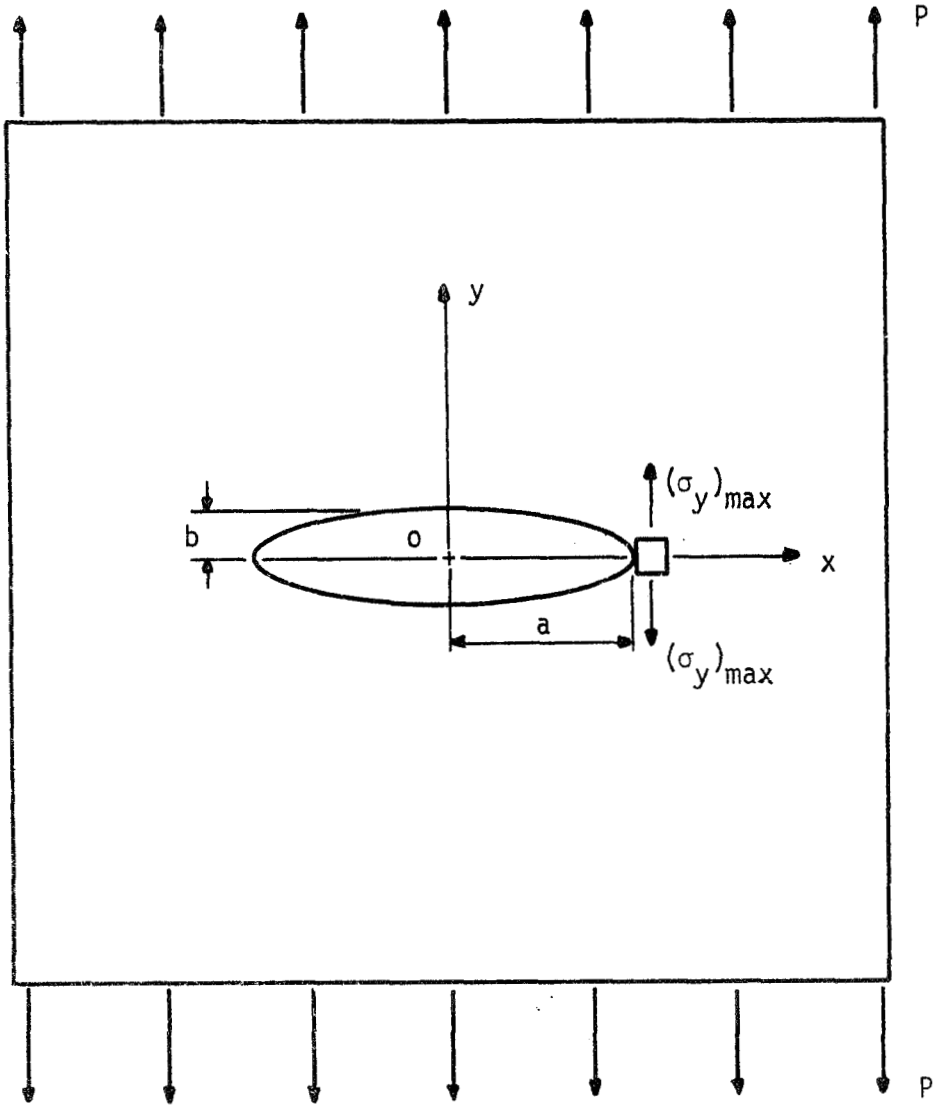

Fig. 1 Uniaxial Tension of Elliptical Hole.

very narrow ellipse or crack of length 2a having a notch radius of curvature $R = b^2/a$, the stress concentration is approximately given by

$$(\sigma_y)_{max} = 2P(a/R)^{1/2} \tag{1.2.2}$$

Since R is very small when compared to a, the actual stress at the root of the crack could be sufficiently large to cause fracture.

The classical treatment of the fracture problem is due to Griffith [7] who approached the question by appealing to the first law of thermodynamics. He postulated that a necessary condition for a crack to extend under the influence of external loads is that the energy Q used in creating new fracture surface is supplied from the released strain energy W in the elastic solid and that $W \geq Q$ in order for the crack to extend. Griffith assumed that the free surface of a solid possessed a surface energy in proportion to its area just as liquids possess surface tension. The knowledge of the elastic energy stored in a loaded cracked solid was a prerequisite for determining the instability condition for crack propagation. Griffith's calculation for the change in strain energy W of an elastic body due to the presence of a crack was based on Inglis' solution for an elliptical hole in a stressed body. It should be mentioned that both Q and W depend on the size of the crack. According to Griffith, the stationary value of the free energy $F = Q - W$ corresponds to a certain critical crack length a_{cr}. Referring to Fig. 2, Griffith's energy criterion assumes that crack extension takes place when a, the half crack length, exceeds the critical value a_{cr}. In addition, if the surface energy of the

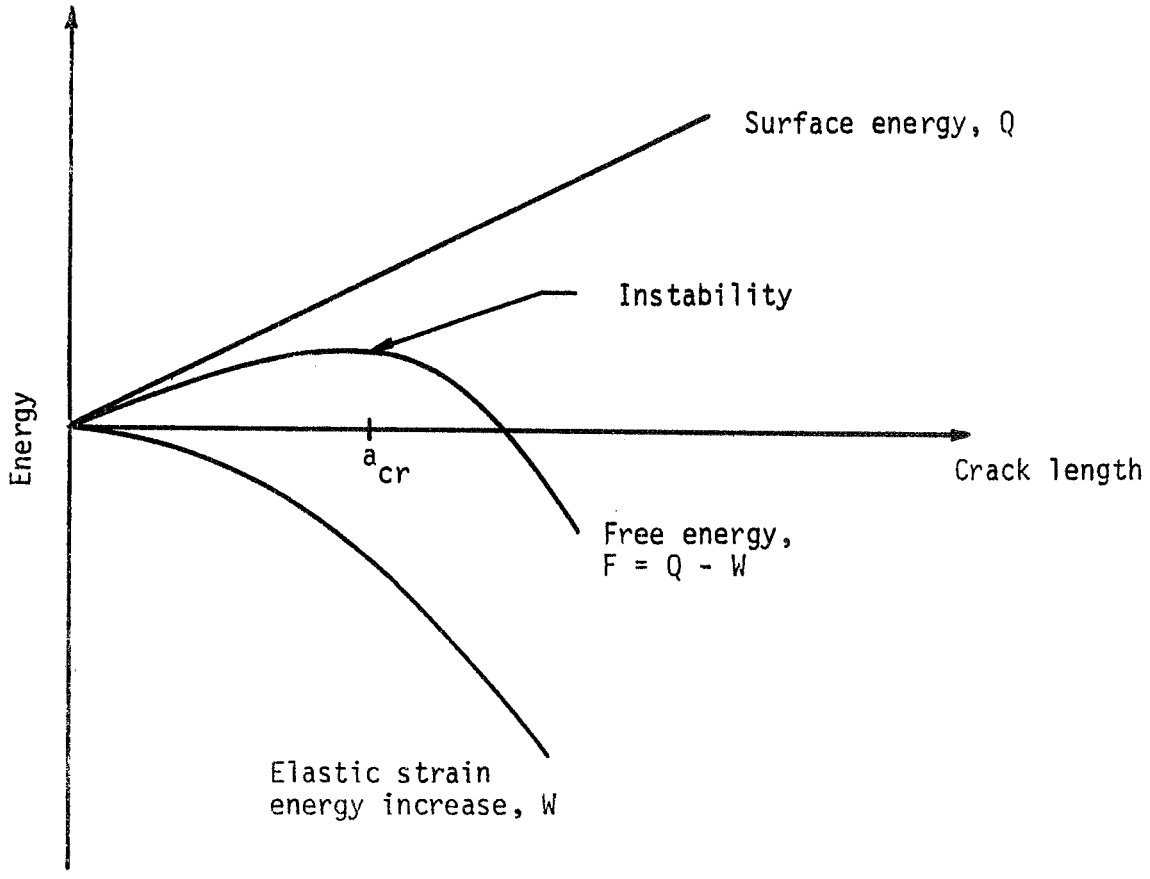

Fig. 2 Energy Balance of Crack in Infinite Plate.

material and crack size are known, the failure criterion can yield an inequality defining the minimum load for fracture. The results of Griffith's theory were well supported by his own experiments on hard glass, but he specifically excluded ductile materials.

Subsequent theories have largely dealt with modifications and generalizations of Griffith's work. In general terms, the energy balance criteria are based on the thermodynamic notion that when the rate of release of stored strain energy exceeds the sum of the rates of absorption of energy in producing plastic deformation and newly created fracture surface, then the crack will extend [5]. Due to the generality and flexibility as well as the physical soundness of this underlying principle, the energy balance approach forms the basis for the most widely used theories of fracture.

Sack [8] in 1946 extended Griffith's work to the three dimensional case. He calculated the conditions of fracture for a solid containing a circular or penny-shaped crack when one of the principal stresses is acting normal to the plane of the crack. Sneddon [9] using cylindrical polar coordinates and the theory of Hankel transforms arrived at the displacements and stresses around a circular crack of the type introduced by Sack.

In the late 1940's and early 1950's Irwin [10] and Orowan [11] independently offered a modification of the Griffith-type energy balance to include plastic work as an additional source of energy dissipation. They pointed out that the energy balance approach must include not only the strain energy stored in the specimen and the surface energy but also the work in plastic deformation. They recognized that for relatively

ductile materials the work done against surface tension is generally not significant in comparison with the work done against plastic deformation. This modification extended the usefulness of the theory to the fracture of metallic materials.

In the energy balance theories, the rate of release of strain energy with respect to fracture area called tear energy, fracture energy or fracture toughness plays an important role. It is considered to be an intrinsic property of the material and is dependent on environmental conditions, type of loading, as well as the nature and composition of the material.

Between 1955 and 1957 Irwin [12, 13] demonstrated that the energy balance approach is equivalent to a stress-intensity approach. Instead of considering the energy of the entire crack system, Irwin proposed to examine the stress field immediately in the vicinity of the crack. Using Sneddon's result [9] for the stress distribution around a circular crack, he pointed out that the crack tip stresses due to the conditions of generalized plane stress or plane strain can be expressed by a parametric set of equations. The parameter, called stress-intensity factor, is a function of the crack dimensions and external loads. The critical value of the stress-intensity factor (determined experimentally for different materials) governs the condition of unstable crack propagation. A typical curve illustrating those combinations of applied stress and crack length at the onset of rapid crack extension is shown in Fig. 3.

Sanders [14] in 1960, in an attempt to establish the equivalence of the energy and stress criteria for fracture, reformulated the two-

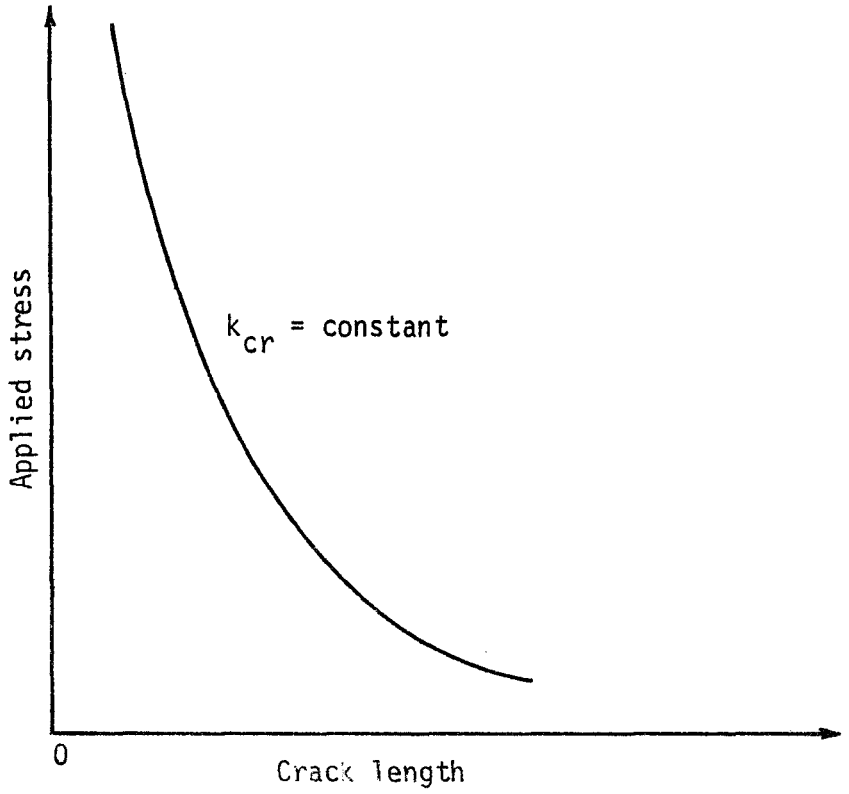

Fig. 3 Stress-Intensity Factor Curve.

dimensional theory of Griffith and obtained an equivalent criterion involving a particular integral around any contour enclosing the crack tip. His result suggests that for crack growth to occur, the energy criterion for fracture is potentially equivalent to postulating the existence of a critical strength of an inverse square root stress singularity [15].

It should be mentioned that a mathematical solution for a sharp crack in a plate using linear elasticity theory predicts singular stresses at the crack tip where the radius of curvature is assumed to be zero. Of course in reality, the deformed shape of the crack adopts a small but finite curvature at the tip, and the stress levels are smaller in magnitude than some ultimate stress. In addition, the occurrence of local plastic flow also tends to reduce the stress-concentrating effect of the crack.

Barenblatt [16], objecting to the idea of infinite stresses at the crack tip, has introduced the effect of cohesive forces acting across the faces of the crack close to its tips. He formulated the following hypotheses:

(1) The end region in which the cohesive forces act is "very small" in comparison with the crack length.

(2) The stresses at the crack tip are finite.

(3) The crack surfaces close smoothly, in other words the crack tip has a cusp shape as depicted in Fig. 4 rather than being parabolic as predicted by the elastic theory.

The cohesive forces pull the crack faces together, and taken by themselves (i.e. no remote tension applied), they induce compressive stress

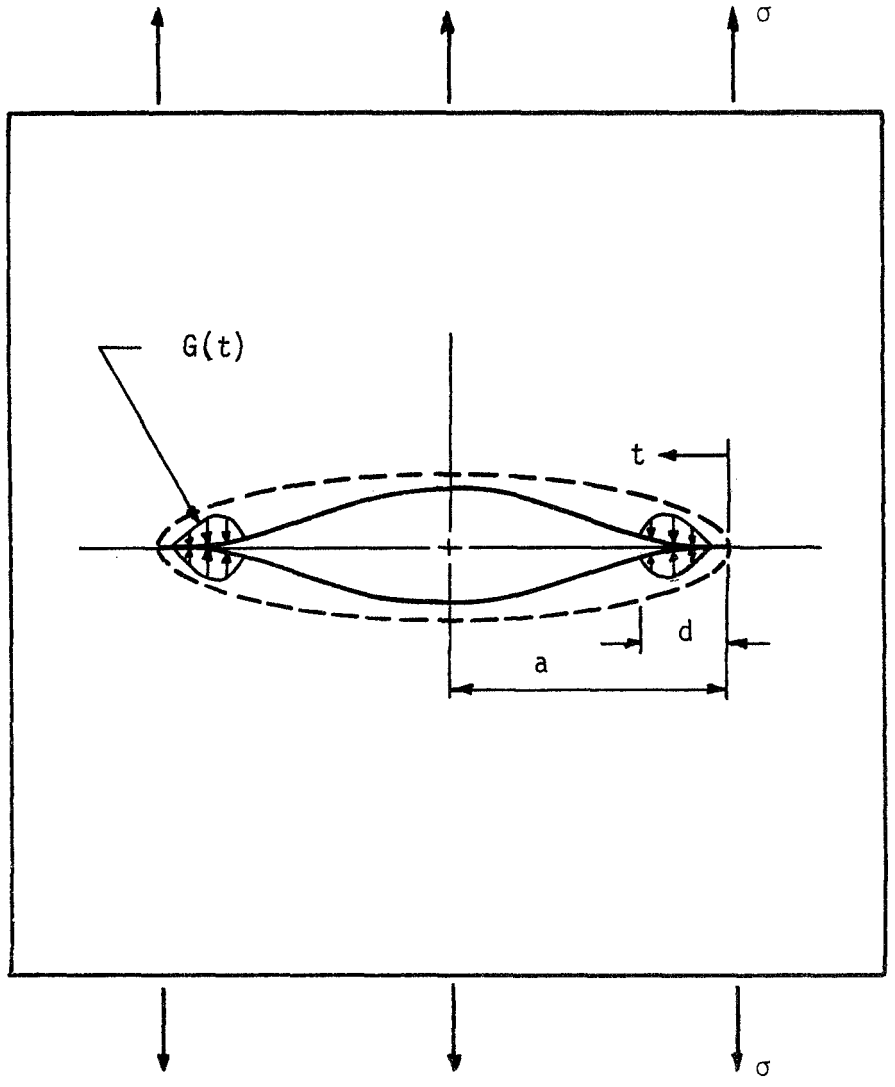

Fig. 4 Cohesive Forces at Crack Tip in the Barenblatt Theory.

singularities at the ends. On the other hand the remote tension alone induces a tensile singularity, and the superposition of the two stress states results in a final stress state that is non-singular. Barenblatt thus obtains a fracture criterion by writing the combined stress intensity factor equal to zero. The result is the comparison of the stress intensity factor calculated from the external loads with a material parameter called the modulus of cohesion. The cohesive modulus N is given by

$$N = \int_0^d \frac{G(t)\, dt}{\sqrt{t}} \qquad (1.2.3)$$

where G(t) is the cohesive force distribution, d is the distance over which this distribution acts ($d << a$), and t is a running coordinate along the x-axis, see Fig. 4. Barenblatt never specified the particular form of G(t). Barenblatt's theory is similar to that of Griffith's and leads to identical results differing only in its interpretation of the stress and deformation states at the crack tip.

In the theories of Griffith and Barenblatt, the idealized media remain linearly elastic as the crack extends, and there is no real expectation that they can represent crack extension in normally ductile materials. A crack in a ductile material has zones of plastic flow at each end during an early stage of loading, and these zones grow as the load is increased. The corresponding problems of the elastic-plastic continuum are very formidable, and only a few results are available (see Hutchinson [17, 18], and Rice and Rosengren [19]).

An important step towards a description of plastic yielding at a

crack tip was introduced by Dugdale [20]. Dugdale's approach, as will be detailed subsequently, was similar to that of Barenblatt, but he replaced the unknown cohesive force distribution G(t) by the known uniaxial yield stress of the material. His experimental results on mild steel for the size and shape of the plastic zone indicate good correlation with theory. Utilizing the results of Dugdale, Goodier and Field [21] were able to evaluate the plastic energy dissipation using the methods of elastic perfectly-plastic continuum mechanics.

As is evidenced by the nature of the literature cited thus far, considerable effort has been expended in studying the brittle and ductile fracture of metals. Reference [22] offers a comprehensive review of the analytical and experimental techniques, as well as an extensive bibliography on the fracture of metals. While much has been written about the fracture of metals, relatively little attention has been directed toward studying the fracture of polymers.

There is an abundance of scientific literature concerning the synthesis and structure of polymers, but the physics of their properties has not been dealt with as extensively. It is only recently, as engineers are becoming increasingly interested in structural applications for polymers that the gaps in our physical understanding of these materials are being exposed. It is not sufficient to rely on past experience with other solids such as metals because polymers often exhibit unfamiliar and unexpected properties.

As previously mentioned, the energy balance approach serves as a basis for much of the work that has been accomplished in fracture mechanics. In an effort to extend this concept to polymeric materials,

the logical place to begin is with glassy polymers since they behave in a brittle fashion and viscoelastic effects can be minimized due to their high glass transition temperatures. Berry [23, 24] has investigated the behavior of polymethyl methacrylate and polystyrene and found that the failure stress as a function of crack length obeyed the inverse square root law of brittle fracture. Broutman and McGarry [25, 26] have studied the effects of temperature, cross linking, and preorientation on the fracture energy of glassy polymers. Lindsey [27] and Andrews [28] offer well documented sources on the fracture of polymers. Very little research has been conducted on ductile polymers. It has only recently been demonstrated by Brinson [29] that the Dugdale mathematical model can be applied to the ductile fracture of polymers.

1.3 Scope of this Investigation

This investigation is basically divided into two parts, an analytical portion and an experimental portion. These aspects will be briefly indicated at this point and then detailed subsequently.

The analytical portion concerns an extension of the isotropic Dugdale mathematical model [20]. The familiar Dugdale model assumes a plastic zone to exist in front of the crack that is a thin extension of the crack line. Experimental investigations [29] [30] on certain materials reveal that the plastic zone is candle-flame shaped and appears to originate, not at the crack tip, but slightly adjacent to it, and proceed initially in a direction other than the crack line. It is felt that a possible cause for the initial shape of the plastic zone is the stress state near a crack tip. If this is the case, then

admissible stress states might exist other than that normally assumed for the Dugdale model (a tensile yield stress normal to the crack line on the elastic-plastic interface). It is proposed to modify the Dugdale model by assuming the existence of a uniform shear stress acting along the plastic zone boundary. Such a modification might alter the stress distribution sufficiently to cause plastic zones to be different than those predicted by the Dugdale model. A solution to this problem has been obtained, and a comparison between Dugdale's work and the results of this solution is presented.

The experimental aspect deals with a verification of the Dugdale model applied to an anisotropic plate as presented by Gonzalez [31]. This approach assumes that differing plastic zone shapes occur due to material properties, i.e. local anisotropy. Gonzalez's analytical solution also discusses the effect of the Mises yield criterion on the anisotropic problem and presents limits on the applicability of the yield criterion depending on the anisotropic properties of the material. The experimental effort has been directed towards verifying some of the predictions of Gonzalez's solution.

The unifying consideration that prompted both the analytical and experimental portions of this investigation was to study the plastic behavior that is characteristic in the fracture of ductile materials. The analytical solutions of Gonzalez and the modified Dugdale model that is presented subsequently were motivated by a desire to more fully understand the nature of the plastic flow that has been observed in ductile materials. In other words, why do plastic zone sizes and shapes vary from material to material? For example, the localized

yielding of the Dugdale type appears to be valid only for materials whose stress-strain behavior is closely approximated as rigid perfectly-plastic while other materials exhibit more diffuse flow patterns. It is hoped that this effort will assist in answering some of the questions associated with these problems.

CHAPTER II

MODIFIED DUGDALE MODEL

While investigating the yielding of steel sheets containing slits, Dugdale [20] observed that the yielded region was shaped as a thin extension of the crack. He formulated the following three hypotheses:

1. The material in the yielded zone is under a uniform tensile yield stress Y, see Fig. 5.
2. The yielded zone is a thin extension of the crack line such that the material outside the zone is elastic and is bounded by a flattened ellipse of length $2a = 2(\ell + s)$, where ℓ is the half crack length and s is the length of the plastic zone, see Fig. 6.
3. The length s is such that there is no stress singularity at the ends of the flattened ellipse.

In addition to these hypotheses, it is proposed that:

4. The material in the yielded zone is under a uniform shear stress T, see Fig. 7.

It might be wise to briefly point out some justification for the fourth assumption stated above.

If one examines the work of Brinson [29], it is noted that the initial yielding that occurs in polycarbonate appears to start at some point slightly removed from the crack tip, see Fig. 8. It was thought that the introduction of a uniform shear stress along the yielded zone in the Dugdale model might give rise to a situation where the

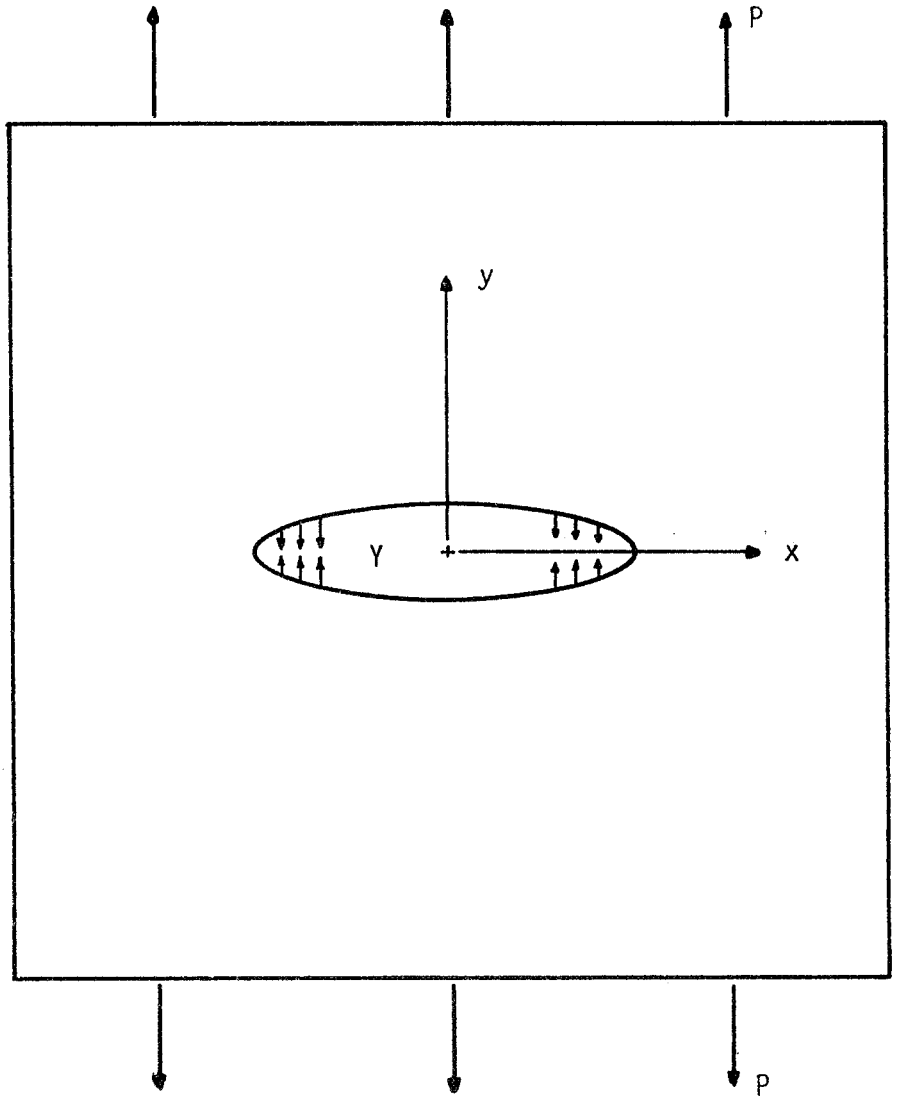

Fig. 5 Plastic Zone Replaced by Yield Stress.

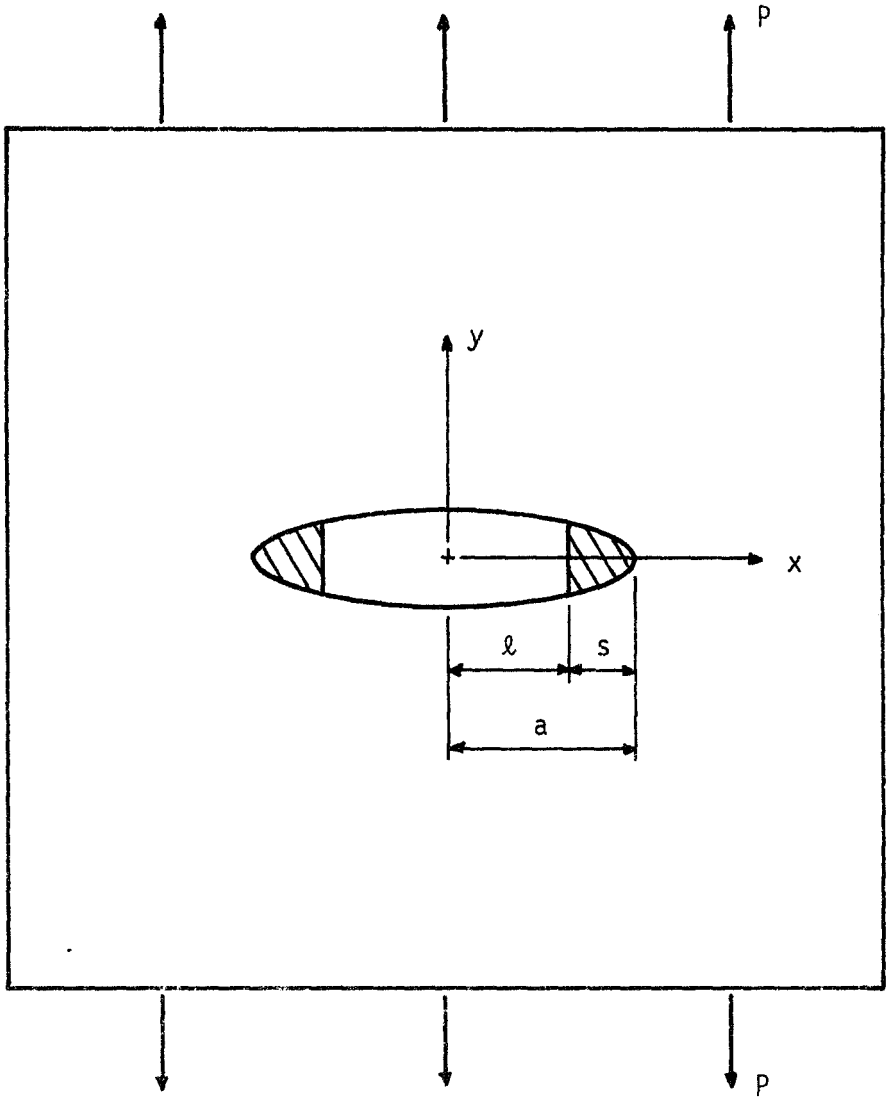

Fig. 6 **Dugdale Model.**

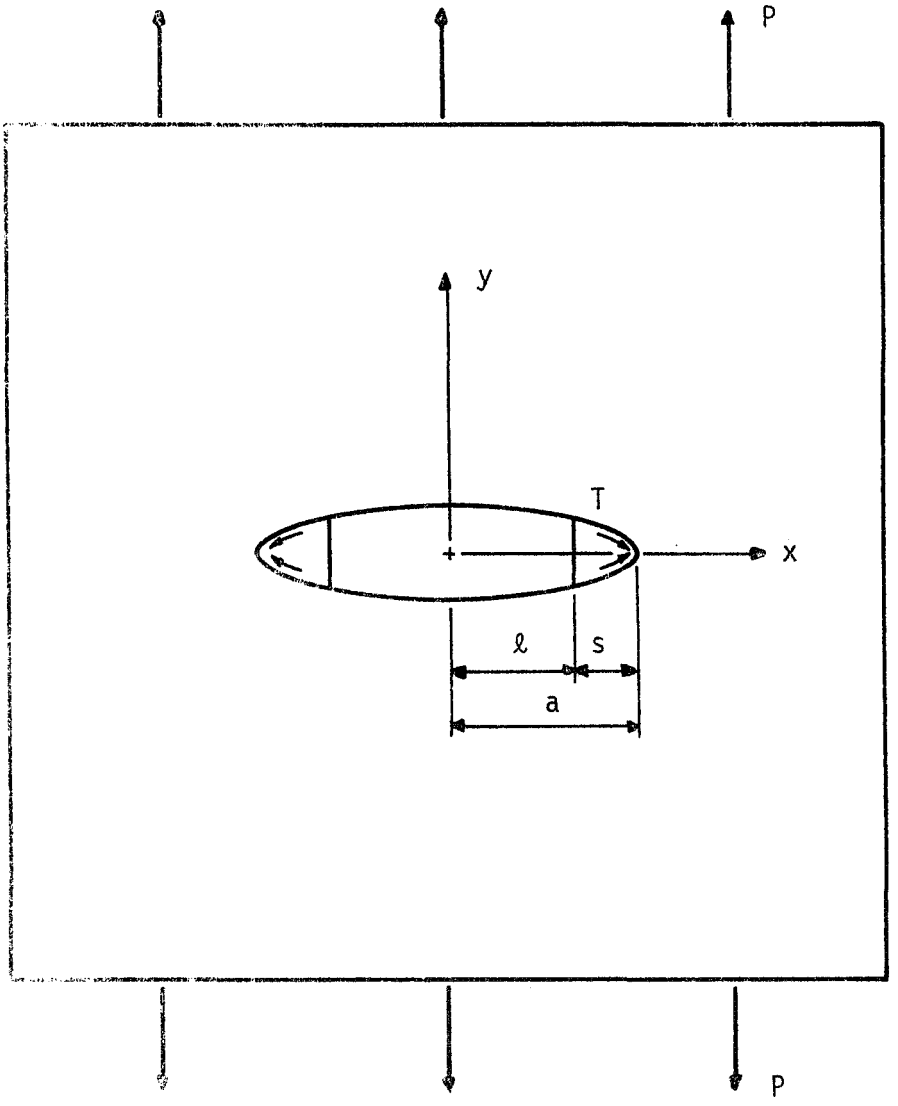

Fig. 7 Dugdale Model with Shear Stress.

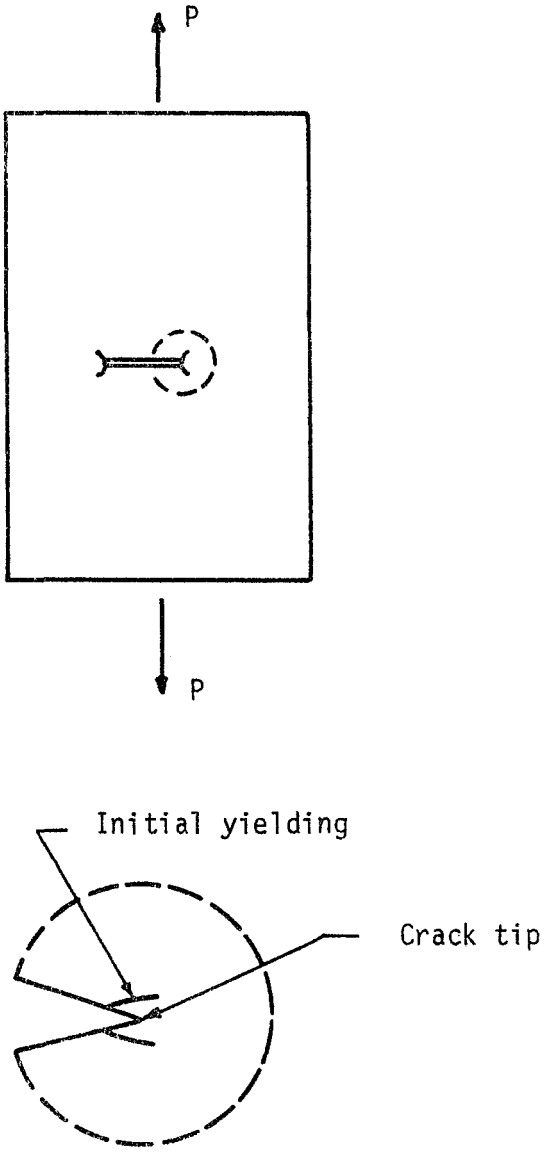

Fig. 8 Initial Yielding in Polycarbonate.

maximum stress state did not occur at the crack tip but at some adjacent point and thereby obtain a plastic zone of a different shape than Dugdale's. In other words, yielding would presumably initially proceed in a direction other than the crack line. As previously mentioned other investigators have reported plastic zone shapes that resemble a candle flame. If the state of stress in the neighborhood of a crack tip is responsible for the initial shape of the plastic zone, then the proposed modification might alter the stress distribution sufficiently so as to predict a plastic zone that differs from the Dugdale type.

Another reason for the addition of the uniform shear stress to the Dugdale model was the desire to realize more complex stress states along the elastic-plastic boundary other than just uniaxial tension. This is in contrast to the ligament type model adopted by Goodier and Kanninen [32]. It was hoped that this modification of the Dugdale model would illustrate the possibility of a more complex stress state existing along the elastic-plastic boundary.

A solution to this boundary value problem can be obtained using the complex variable formulation of Muskhelishvili [33]. The technique for solution involves the superposition of several stress functions corresponding to the component stress states for the modified Dugdale crack, see Fig. 9. The problem then reduces to the following: Given an infinitely large elastic isotropic sheet containing an elliptical hole with specified forces acting on the contour of the hole, what are the stress functions for this particular geometry? Superposing the stress states shown in Fig. 9, and taking the limit as the ellipse flattens to a crack gives the stress distribution for our model.

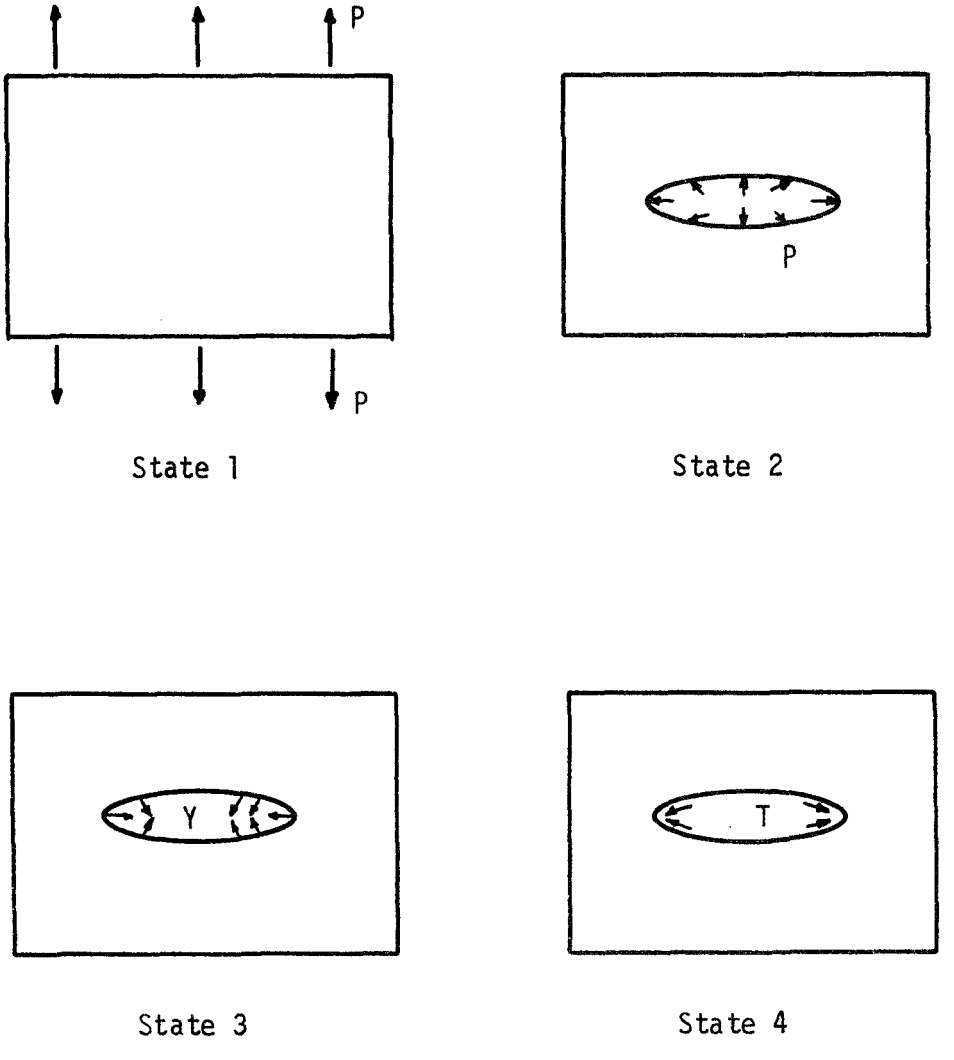

Fig. 9 Component Stress States for Modified Dugdale Crack.

Muskhelishvili [33] gives the following stress functions to solve the problem of an infinite sheet containing an elliptical hole which is loaded over a portion of its boundary by a uniform normal stress as shown in Fig. 10.

$$\phi(\zeta) = \frac{P}{2\pi i}\left\{ - \frac{ma}{2\zeta} \log \frac{\sigma_2}{\sigma_1} + \left[\frac{a}{2}\left(\zeta + \frac{m}{\zeta}\right) - z_2 \right] \log (\sigma_2 - \zeta) \right.$$

$$\left. - \left[\frac{a}{2}\left(\zeta + \frac{m}{\zeta}\right) - z_1 \right] \log (\sigma_1 - \zeta) - \frac{\kappa (z_1 - z_2)}{1 + \kappa} \log \zeta \right\} \tag{2.1}$$

$$\psi(\zeta) = \frac{P}{2\pi i}\left\{ - \frac{a}{2} \frac{(1 + m^2)}{\zeta^2 - m} \zeta \log \frac{\sigma_2}{\sigma_1} + \frac{a}{2} (\sigma_1 - \sigma_2) \frac{1 + m\zeta^2}{\zeta^2 - m} \right.$$

$$- \bar{z}_2 \log (\sigma_2 - \zeta) + \bar{z}_1 \log (\sigma_1 - \zeta) - \frac{(\bar{z}_1 - \bar{z}_2)}{1 + \kappa} \cdot$$

$$\left. \log \zeta - \frac{(z_1 - z_2)}{1 + \kappa} \frac{1 + m^2}{\zeta^2 - m} \right\}$$

where

$$z = \omega(\zeta) = \frac{a}{2}\left(\zeta + \frac{m}{\zeta}\right)$$

$$z_1 = \frac{a}{2}\left(\sigma_1 + \frac{m}{\sigma_1}\right), \qquad z_2 = \frac{a}{2}\left(\sigma_2 + \frac{m}{\sigma_2}\right) \tag{2.2}$$

$$\kappa = \frac{3 - \nu}{1 + \nu} \quad \text{(for plane stress)}$$

$$z = x + iy$$

For state 2 as shown in Fig. 9, the stress functions in (2.1) reduce to

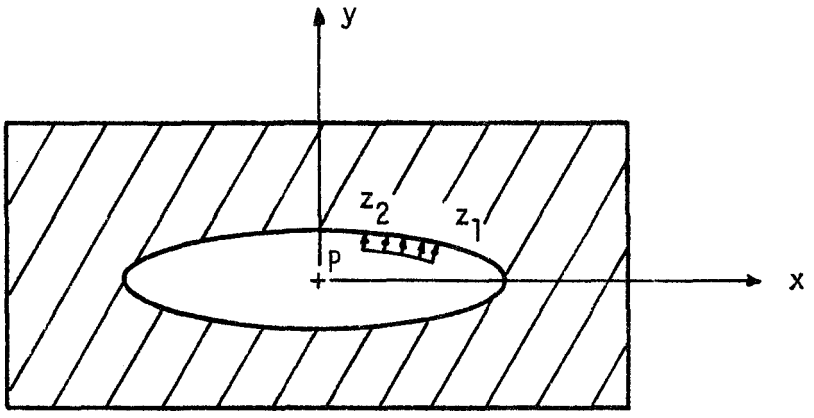

Real plane

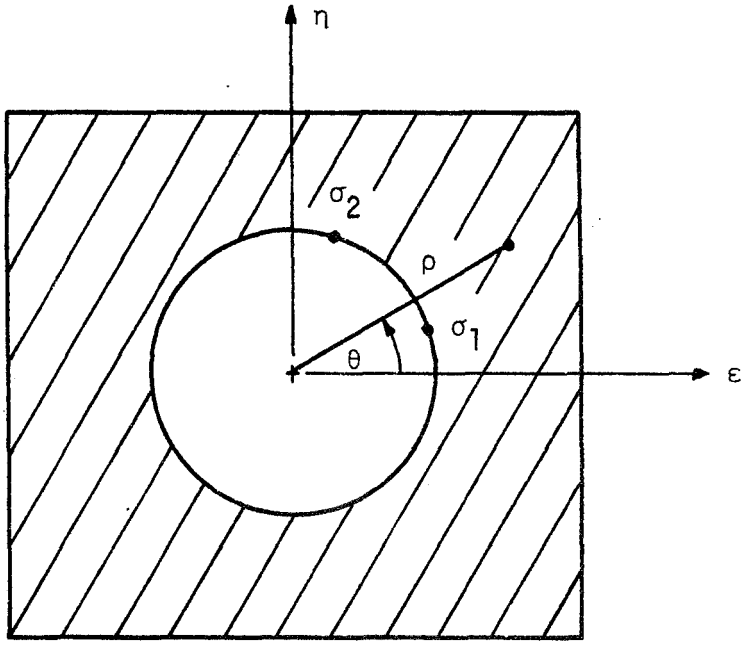

Conformal plane

Fig. 10 Coordinate Systems.

$$\phi_2(\zeta) = -\frac{Pa}{2\zeta}$$

$$\psi_2 = -\frac{Pa\zeta}{\zeta^2 - 1} \tag{2.3}$$

for the limiting case where the ellipse flattens to a crack (m = 1). The above reduction is easily made from (2.1) by taking $z_1 = z_2$. For state 3 in Fig. 9 the stress functions in (2.1) lead to

$$\phi_3(\zeta) = \frac{\gamma}{2\pi i}\left\{-\frac{2ia\theta_2}{\zeta} + \frac{a}{2}\left(\zeta + \frac{1}{\zeta}\right)\log\frac{(\sigma_2 - \zeta)(\sigma_2 + \zeta)}{(\overline{\sigma}_2 - \zeta)(\overline{\sigma}_2 + \zeta)} + \ell\log\frac{(\overline{\sigma}_2 - \zeta)(\sigma_2 + \zeta)}{(\sigma_2 - \zeta)(\overline{\sigma}_2 + \zeta)}\right\}$$

$$\psi_3(\zeta) = \frac{-\gamma}{2\pi i}\left\{-\frac{4ia\theta_2\zeta}{\zeta^2 - 1} + \ell\log\frac{(\overline{\sigma}_2 - \zeta)(\sigma_2 + \zeta)}{(\sigma_2 - \zeta)(\overline{\sigma}_2 + \zeta)}\right\} \tag{2.4}$$

for the limiting case (m = 1), where $\sigma_2 = e^{i\theta_2}$ and $\ell/a = \cos\theta_2$.

In order to determine the stress functions for state 4 as pictured in Fig. 9, which corresponds to an infinite sheet containing an elliptical hole loaded over a portion of its boundary by a uniform shear stress, it was necessary to derive them in a general form using the method presented by Muskhelishvili [33]. The appropriate stress functions are

$$\phi(\zeta) = -\frac{T}{2\pi}\left\{-\frac{am}{2\zeta}\log\frac{\sigma_2}{\sigma_1} + \left[\frac{a}{2}\left(\zeta + \frac{m}{\zeta}\right) - z_2\right]\log(\sigma_2 - \zeta)\right.$$

$$\left. - \left[\frac{a}{2}\left(\zeta + \frac{m}{\zeta}\right) - z_1\right]\log(\sigma_1 - \zeta) - \frac{\kappa(z_1 - z_2)}{\kappa + 1}\log\zeta\right\}$$

(2.5)

$$\psi(\zeta) = \frac{T}{2\pi}\left\{\left[-\frac{a}{2\zeta} + \frac{am}{2\zeta}\frac{(1 + m\zeta^2)}{(\zeta^2 - m)}\right]\log\frac{\sigma_2}{\sigma_1} + a\left(m\zeta + \frac{1}{\zeta}\right)\log\frac{(\sigma_2 - \zeta)}{(\sigma_1 - \zeta)}\right.$$

$$- \frac{a}{2}(\sigma_1 - \sigma_2)\frac{(1 + m\zeta^2)}{(\zeta^2 - m)} - \bar{z}_2\log(\sigma_2 - \zeta) + \bar{z}_1\log(\sigma_1 - \zeta)$$

$$\left. - \frac{(\bar{z}_1 - \bar{z}_2)}{(1 + \kappa)}\log\zeta\right\}$$

where the variables z, z_1, z_2, and the constant κ are defined in equation (2.2). In order to arrive at the particular form of the desired stress functions it might be helpful to refer to Fig. 11 where the variables that define the limits of application of the uniform shear stress are shown. Upon making the appropriate substitutions into equations (2.5) for the loading shown in Fig. 11, the corresponding stress functions are given by

$$\phi_4(\zeta) = \frac{T}{2\pi}\left\{\frac{a}{2}\left(\zeta + \frac{1}{\zeta}\right)\log\frac{(\sigma_2 - \zeta)(\bar{\sigma}_2 - \zeta)(\sigma_2 + \zeta)(\bar{\sigma}_2 + \zeta)}{(1 + \zeta)^2(1 - \zeta)^2}\right.$$

$$\left. + \ell\log\frac{(\sigma_2 + \zeta)(\bar{\sigma}_2 + \zeta)}{(\sigma_2 - \zeta)(\bar{\sigma}_2 - \zeta)} + 2a\log\frac{(1 - \zeta)}{(1 + \zeta)}\right\}$$

(2.6)

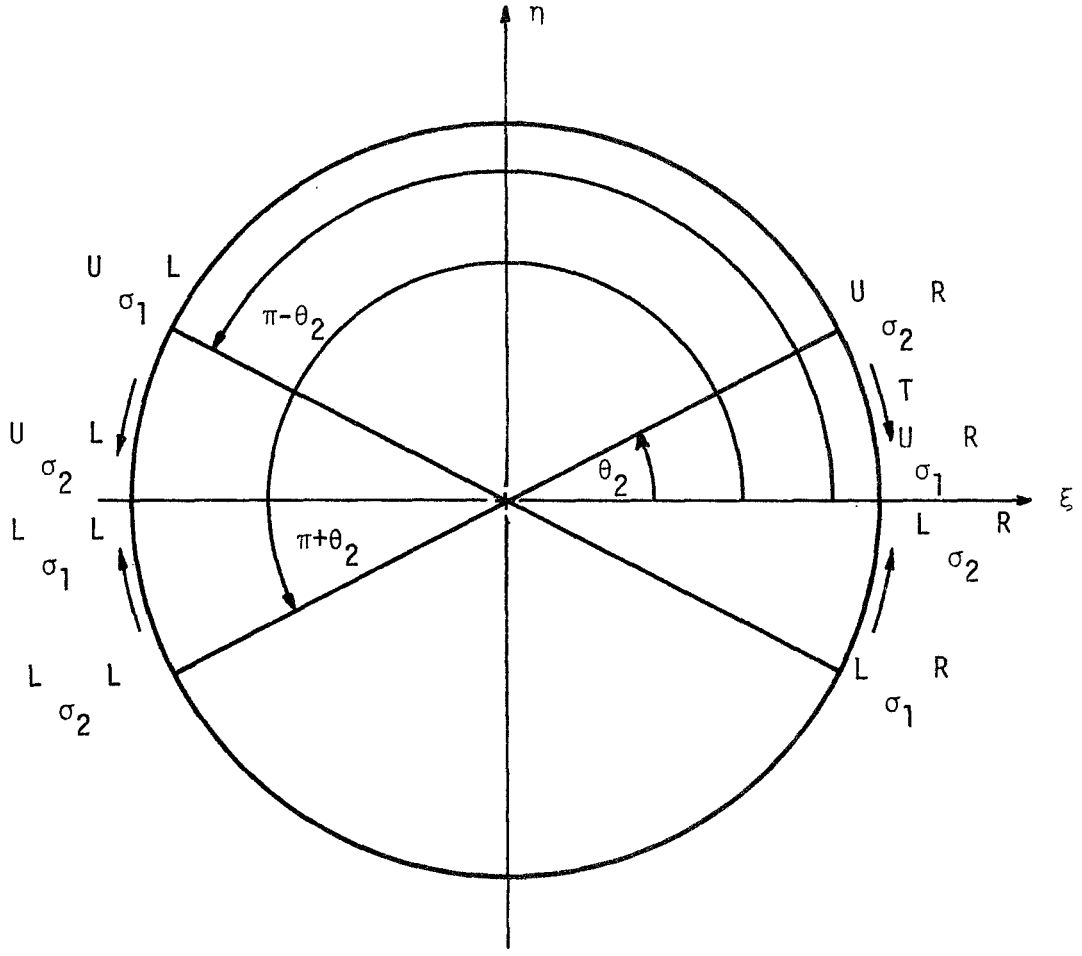

$$\overset{U\ R}{\sigma_1} = 1 \qquad \overset{L\ L}{\sigma_1} = -1$$

$$\overset{U\ R}{\sigma_2} = \sigma_2 \qquad \overset{L\ L}{\sigma_2} = -\sigma_2$$

$$\overset{U\ L}{\sigma_1} = -\bar{\sigma}_2 \qquad \overset{L\ R}{\sigma_1} = \bar{\sigma}_2$$

$$\overset{U\ L}{\sigma_2} = -1 \qquad \overset{L\ R}{\sigma_2} = 1$$

Fig. 11 Loading in Conformal Plane.

$$\psi_4(\zeta) = \frac{T}{2\pi}\left\{ a\left(\zeta + \frac{1}{\zeta}\right)\log\frac{(1+\zeta)^2(1-\zeta)^2}{(\overline{\sigma}_2+\zeta)(\overline{\sigma}_2-\zeta)(\sigma_2+\zeta)(\sigma_2-\zeta)} + \ell\log\frac{(\sigma_2-\zeta)(\overline{\sigma}_2-\zeta)}{(\sigma_2+\zeta)(\overline{\sigma}_2+\zeta)} + 2a\log\frac{(1+\zeta)}{(1-\zeta)}\right\}$$

for the limiting case (m = 1), and where σ_2 and ℓ are as previously defined.

Superposing the stress functions in (2.3), (2.4), and (2.6) which correspond to stress states 2, 3, and 4 in Fig. 9 yields the following

$$\begin{aligned}\phi(\zeta) = {} & \frac{a}{\zeta}\left\{\frac{\gamma\theta_2}{\pi} - \frac{P}{2}\right\} - \frac{\gamma}{2\pi i}\left\{\frac{a}{2}\left(\zeta+\frac{1}{\zeta}\right)\log\frac{(\sigma_2-\zeta)(\sigma_2+\zeta)}{(\overline{\sigma}_2-\zeta)(\overline{\sigma}_2+\zeta)}\right. \\ & \left. + \ell\log\frac{(\overline{\sigma}_2-\zeta)(\sigma_2+\zeta)}{(\sigma_2-\zeta)(\overline{\sigma}_2+\zeta)}\right\} + \frac{T}{2\pi}\left\{\frac{a}{2}\left(\zeta+\frac{1}{\zeta}\right)\cdot\right. \\ & \log\frac{(\sigma_2-\zeta)(\overline{\sigma}_2-\zeta)(\sigma_2+\zeta)(\overline{\sigma}_2+\zeta)}{(1+\zeta)^2(1-\zeta)^2} \\ & \left. + \ell\log\frac{(\overline{\sigma}_2+\zeta)(\sigma_2+\zeta)}{(\overline{\sigma}_2-\zeta)(\sigma_2-\zeta)} + 2a\log\frac{(1-\zeta)}{(1+\zeta)}\right\}\end{aligned} \tag{2.7}$$

$$\begin{aligned}\psi(\zeta) = {} & \frac{2a\zeta}{\zeta^2-1}\left\{\frac{\gamma\theta_2}{\pi} - \frac{P}{2}\right\} - \frac{\gamma}{2\pi i}\left\{\ell\log\frac{(\overline{\sigma}_2-\zeta)(\sigma_2+\zeta)}{(\overline{\sigma}_2+\zeta)(\sigma_2-\zeta)}\right\} \\ & + \frac{T}{2\pi}\left\{a\left(\zeta+\frac{1}{\zeta}\right)\log\frac{(1+\zeta)^2(1-\zeta)^2}{(\overline{\sigma}_2+\zeta)(\sigma_2+\zeta)(\overline{\sigma}_2-\zeta)(\sigma_2-\zeta)}\right. \\ & \left. + \ell\log\frac{(\sigma_2-\zeta)(\overline{\sigma}_2-\zeta)}{(\sigma_2+\zeta)(\overline{\sigma}_2+\zeta)} + 2a\log\frac{(1+\zeta)}{(1-\zeta)}\right\}\end{aligned}$$

It is noted that the expressions for the stress functions above contain singular portions that violate Dugdale's third hypothesis. The leading term corresponds to a dominant singularity of the inverse square root type that is characteristic of linear elastic fracture mechanics. Each expression also contains a weaker logarithmic singularity that influences the effect of the assumed shear stress. Following Dugdale's approach, the dominant singular term is annihilated and this requires that

$$\frac{Y\theta_2}{\pi} - \frac{P}{2} = 0 \tag{2.8}$$

In order to evaluate the influence of the assumed shear stress the weaker logarithmic singularity is retained; therefore, the stress functions corresponding to the modified Dugdale crack (exclusive of the uniform tension field $\sigma_y = P$) reduce to

$$\phi(\zeta) = -\frac{Y}{2\pi i}\left\{\frac{a}{2}\left(\zeta + \frac{1}{\zeta}\right)\log\frac{(\sigma_2 - \zeta)(\sigma_2 + \zeta)}{(\overline{\sigma}_2 - \zeta)(\overline{\sigma}_2 + \zeta)} + \ell \log\frac{(\overline{\sigma}_2 - \zeta)(\sigma_2 + \zeta)}{(\sigma_2 - \zeta)(\overline{\sigma}_2 + \zeta)}\right\}$$

$$+\frac{T}{2\pi}\left\{\frac{a}{2}\left(\zeta + \frac{1}{\zeta}\right)\log\frac{(\sigma_2 - \zeta)(\overline{\sigma}_2 - \zeta)(\sigma_2 + \zeta)(\overline{\sigma}_2 + \zeta)}{(1 + \zeta)^2\,(1 - \zeta)^2}\right.$$

$$\left. + \ell \log\frac{(\sigma_2 + \zeta)(\overline{\sigma}_2 + \zeta)}{(\sigma_2 - \zeta)(\overline{\sigma}_2 - \zeta)} + 2a \log\frac{(1 - \zeta)}{(1 + \zeta)}\right\} \tag{2.9}$$

$$\psi(\zeta) = -\frac{Y}{2\pi i}\left\{ \ell \log \frac{(\bar{\sigma}_2 - \zeta)(\sigma_2 + \zeta)}{(\sigma_2 - \zeta)(\bar{\sigma}_2 + \zeta)} \right\} + \frac{T}{2\pi}\left\{ a\left(\zeta + \frac{1}{\zeta}\right) \cdot \right.$$

$$\log \frac{(1+\zeta)^2 (1-\zeta)^2}{(\bar{\sigma}_2 + \zeta)(\bar{\sigma}_2 - \zeta)(\sigma_2 + \zeta)(\sigma_2 - \zeta)} + \ell \log \frac{(\sigma_2 - \zeta)(\bar{\sigma}_2 - \zeta)}{(\sigma_2 + \zeta)(\bar{\sigma}_2 + \zeta)}$$

$$\left. + 2a \log \frac{(1+\zeta)}{(1-\zeta)} \right\}$$

The displacement components u, v are related by the following equation

$$2\mu(u + i\,v) = \kappa\,\phi(\zeta) - \frac{\omega(\zeta)}{\omega'(\zeta)}\,\overline{\phi'(\zeta)} - \psi(\zeta) \qquad (2.10)$$

We consider next some of the details of the substitution of the stress functions of (2.9) into (2.10) to determine the displacements at the surface of the crack and the elastic-plastic interface on which $\zeta = e^{i\theta}$. It is convenient to consider the terms of (2.10) separately. Since $\sigma_2 = e^{i\theta_2}$, we have

$$\frac{\sigma_2 + \zeta}{\bar{\sigma}_2 + \zeta} = e^{i\theta_2} \frac{\cos\frac{1}{2}(\theta - \theta_2)}{\cos\frac{1}{2}(\theta + \theta_2)} \qquad \frac{\sigma_2 - \zeta}{\bar{\sigma}_2 - \zeta} = e^{i\theta_2} \frac{\sin\frac{1}{2}(\theta - \theta_2)}{\sin\frac{1}{2}(\theta + \theta_2)}$$

$$\frac{\sigma_2 + \zeta}{\sigma_2 - \zeta} = i \cot\frac{1}{2}(\theta - \theta_2) \qquad \frac{\bar{\sigma}_2 + \zeta}{\bar{\sigma}_2 - \zeta} = i \cot\frac{1}{2}(\theta + \theta_2)$$

$$\frac{\sigma_2 + \zeta}{1 + \zeta} = e^{\frac{i\theta_2}{2}} \frac{\cos\frac{1}{2}(\theta - \theta_2)}{\cos\frac{\theta}{2}} \qquad \frac{\bar{\sigma}_2 + \zeta}{1 + \zeta} = e^{\frac{-i\theta_2}{2}} \frac{\cos\frac{1}{2}(\theta + \theta_2)}{\cos\frac{\theta}{2}}$$

(2.11)

$$\frac{\sigma_2 - \zeta}{1 - \zeta} = e^{\frac{i\theta_2}{2}} \frac{\sin \frac{1}{2}(\theta - \theta_2)}{\sin \frac{\theta}{2}} \qquad \frac{\bar{\sigma}_2 - \zeta}{1 - \zeta} = e^{\frac{-i\theta_2}{2}} \frac{\sin \frac{1}{2}(\theta + \theta_2)}{\sin \frac{\theta}{2}}$$

$$\frac{1 + \zeta}{1 - \zeta} = i \cot \frac{\theta}{2}$$

Substituting (2.11) into the expression for $\psi(\zeta)$ in (2.9) and taking the conjugate we find

$$\begin{aligned}\overline{\psi(\zeta)} = &- \frac{iYa}{2\pi} \{ \cos \theta_2 \log \left[\frac{\sin \theta + \sin \theta_2}{\sin \theta - \sin \theta_2} \right] \} \\ &+ \frac{Ta}{\pi} \{ \cos \theta \log \left[\frac{\sin^2 \theta}{\sin^2 \theta - \sin^2 \theta_2} \right] \qquad (2.12) \\ &+ \frac{\cos \theta_2}{2} \log \left[\frac{\cos \theta - \cos \theta_2}{\cos \theta + \cos \theta_2} \right] + \log \left[\frac{\cos \frac{\theta}{2}}{\sinh \frac{i\theta}{2}} \right] \}\end{aligned}$$

The expression for $\phi(\zeta)$ in (2.9) becomes

$$\begin{aligned}\phi(\zeta) = &- \frac{Ya}{2\pi i} \{ 2i \theta_2 \cos \theta + (\cos \theta + \cos \theta_2) \log \left[\frac{\cos \frac{1}{2}(\theta - \theta_2)}{\cos \frac{1}{2}(\theta + \theta_2)} \right] \\ &+ (\cos \theta - \cos \theta_2) \log \left[\frac{\sin \frac{1}{2}(\theta - \theta_2)}{\sin \frac{1}{2}(\theta + \theta_2)} \right] \} \\ &+ \frac{Ta}{2\pi} \{ \cos \theta \log \left[\frac{\sin^2 \theta - \sin^2 \theta_2}{\sin^2 \theta} \right] \qquad (2.13) \\ &+ \cos \theta_2 \log \left[\frac{\cos \theta + \cos \theta_2}{\cos \theta - \cos \theta_2} \right] + 2 \log \left[- i \tan \frac{\theta}{2} \right] \}\end{aligned}$$

Now,

$$\phi'(\zeta) = \frac{d\phi}{d\theta}\,\frac{d\theta}{d\zeta} = -\,i\,e^{-i\theta}\,\frac{d\phi}{d\theta} \tag{2.14}$$

so from (2.13) we have

$$\phi'(\zeta) = -\frac{Yae^{-i\theta}}{2\pi}\left\{ 2i\,\theta_2 \sin\theta + \sin\theta \log\left[\frac{\sin(\theta - \theta_2)}{\sin(\theta + \theta_2)}\right]\right\}$$

$$+\frac{Taie^{-i\theta}}{2\pi}\left\{ \sin\theta \log\left[\frac{\sin^2\theta - \sin^2\theta_2}{\sin^2\theta}\right]\right\} \tag{2.15}$$

The conjugate of this is

$$\overline{\phi'(\zeta)} = -\frac{Yae^{i\theta}}{2\pi}\left\{ -2i\,\theta_2 \sin\theta + \sin\theta \log\left[\frac{\sin(\theta - \theta_2)}{\sin(\theta + \theta_2)}\right]\right\}$$

$$-\frac{Taie^{i\theta}}{2\pi}\left\{ \sin\theta \log\left[\frac{\sin^2\theta - \sin^2\theta_2}{\sin^2\theta}\right]\right\} \tag{2.16}$$

From the definition of $\omega(\zeta)$

$$\frac{\omega(\zeta)}{\omega'(\zeta)} = i\,e^{-i\theta}\cot\theta \tag{2.17}$$

for $\zeta = e^{i\theta}$. Substituting (2.12), (2.13), (2.16), and (2.17) into (2.10) and equating the real and imaginary parts, we find

$$2\mu u = (1-\kappa)\frac{Ya\,\theta_2\cos\theta}{\pi} - (1+\kappa)\frac{Ta}{\pi}\left\{\frac{\cos\theta_2}{4}\cdot\right.$$

$$\left.\log\left[\frac{\cos\theta - \cos\theta_2}{\cos\theta + \cos\theta_2}\right]^2 - \log\left[\tan\frac{\theta}{2}\right]\right\} \tag{2.18}$$

$$-\frac{(3+\kappa)}{4}\,\frac{Ta}{\pi}\left\{\cos\theta \log\left[\frac{\sin^2\theta}{\sin^2\theta + \sin\theta_2}\right]^2\right\}$$

$$2\mu v = -(1+\kappa)\frac{Ya}{2\pi}\left\{\frac{\cos\theta}{2}\log\left[\frac{\sin(\theta+\theta_2)}{\sin(\theta-\theta_2)}\right]^2\right.$$

$$\left.+\frac{\cos\theta_2}{2}\log\left[\frac{\sin\theta-\sin\theta_2}{\sin\theta+\sin\theta_2}\right]^2\right\}-\frac{Ta}{2}(\kappa-1) \quad (2.19)$$

The stress components along the elastic-plastic boundary where $\zeta = e^{i\theta}$ and $\rho = 1$ are determined by substituting the stress functions in (2.9) into the following equations.

$$\sigma_\rho + \sigma_\theta = 4\,\mathrm{Re}\,\Phi \quad (2.20)$$

$$-\sigma_\rho + \sigma_\theta + 2i\,\tau_{\rho\theta} = \frac{2\zeta^2}{\rho^2\,\overline{\omega'(\zeta)}}\left\{\overline{\omega(\zeta)}\,\Phi'(\zeta) + \psi'(\zeta)\right\} \quad (2.21)$$

where

$$\Phi(\zeta) = \frac{\phi'(\zeta)}{\omega'(\zeta)} \quad (2.22)$$

Now

$$\omega'(\zeta) = i\,a\,e^{-i\theta}\sin\theta \quad (2.23)$$

therefore, substituting (2.15) and (2.23) into (2.22) gives

$$\Phi(\zeta) = -\frac{Y}{2\pi i}\left\{2i\,\theta_2 - \log\left[\frac{\sin(\theta+\theta_2)}{\sin(\theta-\theta_2)}\right]\right\}$$

$$+\frac{T}{\pi}\left\{\log\left[\frac{\sin^2\theta-\sin^2\theta_2}{\sin^2\theta}\right]\right\} \quad (2.24)$$

Since,

$$\Phi'(\zeta) = \frac{d\Phi}{d\theta}\,\frac{d\theta}{d\zeta} = -\,i\,e^{-i\theta}\,\frac{d\Phi}{d\theta} \tag{2.25}$$

then

$$\zeta'(\zeta) = \frac{Ye^{-i\theta}}{2\pi}\left\{\frac{\sin 2\theta_2}{\sin^2\theta - \sin^2\theta_2}\right\} - \frac{Tie^{-i\theta}}{2\pi}\left\{\frac{2\cos\theta\sin^2\theta_2}{\sin\theta(\sin^2\theta - \sin^2\theta_2)}\right\} \tag{2.26}$$

Also

$$\psi'(\zeta) = \frac{Yae^{-i\theta}}{2\pi}\left\{\frac{-\sin 2\theta_2\cos\theta}{\sin^2\theta - \sin^2\theta_2}\right\} - \frac{iTae^{-i\theta}}{\pi}\left\{\frac{-\sin^2\theta_2\cos^2\theta}{\sin\theta(\sin^2\theta - \sin^2\theta_2)} - \sin\theta\log\left[\frac{\sin^2\theta}{\sin^2\theta - \sin^2\theta_2}\right]\right\} \tag{2.27}$$

Substituting (2.24) into (2.20) yields

$$\sigma_\rho + \sigma_\theta = \mathrm{Re}\left[-\frac{2Y}{\pi i}\left\{2i\,\theta_2 - \log\left[\frac{\sin(\theta+\theta_2)}{\sin(\theta-\theta_2)}\right]\right\} + \frac{2T}{\pi}\left\{\log\left[\frac{\sin^2\theta - \sin^2\theta_2}{\sin^2\theta}\right]\right\}\right] \tag{2.28}$$

Substitution of (2.26) and (2.27) into (2.21) gives

$$-\sigma_\rho + \sigma_\theta + 2i\,\tau_{\rho\theta} = -\frac{2T}{\pi}\left\{\log\frac{\sin^2\theta}{\sin^2\theta - \sin^2\theta_2}\right\} \tag{2.29}$$

In order to determine the final form for the stresses it is convenient to examine two separate cases, namely $\theta < \theta_2$ and $\theta > \theta_2$ where θ_2 is defined by equation (2.8).

Case I $\theta < \theta_2$

$$\sigma_\rho = Y - P$$

$$\sigma_\theta = Y - P - \frac{T}{\pi}\left\{ \log \left[\frac{\sin^2 \theta}{\sin^2 \theta - \sin^2 \theta_2} \right]^2 \right\} \tag{2.30}$$

$$\tau_{\rho\theta} = 0$$

Case II $\theta > \theta_2$

$$\sigma_\rho = - P$$

$$\sigma_\theta = - P - \frac{T}{\pi}\left\{ \log \left[\frac{\sin^2 \theta}{\sin^2 \theta - \sin^2 \theta_2} \right]^2 \right\} \tag{2.31}$$

$$\tau_{\rho\theta} = 0$$

It should be recalled that equations (2.30) and (2.31) do not include the remote uniform tension field $\sigma_y = P$.

This solution represents an effort to develop a mathematical model which will predict the size, shape, and direction of plastic zone growth in front of cracks using the Dugdale model as a point of departure. The present solution indicates that Dugdale's finiteness condition (equation (2.8)) remains unchanged only if the logarithmic singularity due to the assumed shear stress is retained in the stress functions. It also demonstrates the admissibility of other stress states along the elastic-plastic boundary of a crack. A comparison for the stresses and displacements along the elastic-plastic interface between Dugdale's solution and the predictions of the modified problem was formulated and these results are presented in Chapter IV.

CHAPTER III

EXPERIMENTAL PROGRAM

The impetus for the experimental program was provided by Gonzalez's analytical solution dealing with the adaptation of the Dugdale model to an anisotropic plate [31]. This analytical approach assumes that various shaped plastic zones might occur due to the properties of the material, i.e. local anisotropy. The following experimental effort has been directed toward a qualitative verification of some of the results of this solution. The details of Gonzalez's solution will not be presented here. Perhaps it would suffice to say that the method is quite similar to the procedure outlined in Chapter II. In other words, the principle of superposition was employed to obtain the complete stress functions for the problem by combining the stress functions (taking into account anisotropy) corresponding to the component stress states for the Dugdale model. The desired stress functions were obtained from Savin [34] where he adapted the complex variable approach of Muskhelishvili [33] to the anisotropic case. Some of the salient features of the solution will be presented as they dictate the nature of the experimental investigation.

Examination of the Gonzalez solution reveals that the effect of anisotropy is to modify each isotropic field equation by a multiplicative constant that is a function of the anisotropic material constants. For example the finiteness condition for the anisotropic case can be written as

$$\frac{Y\theta_2}{\pi} - \frac{P}{2} = 0 \tag{3.1}$$

where Y is some constant having the units of stress (not necessarily the tensile yield stress) acting on the plastic zone boundary that is related to the anisotropic yield properties of the material and the other terms are as previously defined. This is similar to the finiteness condition that results in the isotropic case where Y is usually assumed to be the tensile yield stress of the material.

The stresses along the line of the crack $y \equiv 0$ for the anisotropic case are given by

$$\sigma_x = \frac{2Y\ (\beta_1\beta_2 - \alpha_1\alpha_2)}{\pi}\ \tan^{-1}\ \left(\frac{\sin 2\theta_2}{\varepsilon^2 - \cos 2\theta_2}\right) \tag{3.2}$$

$$\sigma_y = \frac{2Y}{\pi}\tan^{-1}\left(\frac{\sin 2\theta_2}{\varepsilon^2 - \cos 2\theta_2}\right) \tag{3.3}$$

where $x = \frac{a}{2}(\varepsilon + \frac{1}{\varepsilon})$, and the stresses at the tip of the plastic zone are

$$\sigma_x = (\beta_1\beta_2 - \alpha_1\alpha_2)(Y - P) \tag{3.4}$$

$$\sigma_y = Y \tag{3.5}$$

where P is the external load. For the isotropic case the stresses along the line of the crack are

$$\sigma_x = \sigma_y = \frac{2Y}{\pi}\tan^{-1}\left(\frac{\sin 2\theta_2}{\varepsilon^2 - \cos 2\theta_2}\right) \tag{3.6}$$

and the stresses at the tip of the plastic zone are

$$\sigma_x = Y - P \tag{3.7}$$

$$\sigma_y = Y \tag{3.8}$$

The constants α_i and β_i appearing in equation (3.2) are related to the anisotropic elastic constants a_{ij} as defined by Lekhnitskii [35] through the characteristic equation for plane stress

$$a_{11} m^4 - 2a_{16} m^3 + (2a_{12} + a_{66})m^2 - 2a_{26} m + a_{22} = 0 \tag{3.9}$$

whose roots m_i take the form

$$m_i = \alpha_i + i\beta_i \tag{3.10}$$

The corresponding expressions for the displacements for the anisotropic case are noted to be significantly affected by the anisotropy of the material as seen below.

$$u = \frac{2 Y a\theta_2}{\pi} [a_{11} (\alpha_1\alpha_2 - \beta_1\beta_2) - a_{12}] \cos \theta \tag{3.11}$$

$$v = \frac{\gamma a}{(\alpha_1^2 + \beta_1^2)(\alpha_2^2 + \beta_2^2)} \text{ Re } [(a_{22} [\beta_1\beta_2 (\beta_1 + \beta_2)$$

$$+ \alpha_1^2\beta_2 + \alpha_2\beta_1 + i [a_{22} [\alpha_1\alpha_2 (\alpha_1 + \alpha_2) + (\alpha_1\beta_2^2 + \beta_1^2 \alpha_2)$$

$$- a_{26} [(\alpha_1^2 + \beta_1^2)(\alpha_2^2 + \beta_2^2)]]) [2 i \theta_2 \cos \theta$$

$$+ 2 \cos \theta \log \sin (\theta + \theta_2) + \cos \theta_2 \log (\sin \theta_2 - \sin \theta)^2$$

$$- \frac{\cos \theta_2 + \cos \theta}{2} \log (\cos^2 \theta_2 - \cos^2 \theta)^2]] \qquad (3.12)$$

In addition to obtaining the field equations for the stresses and displacements, Gonzalez also discusses the effect of the Mises yield criterion for a Dugdale type solution and presents limits on the validity of the solution depending on material properties. The limits on the application of the solution can be illustrated in the following manner. In the isotropic Dugdale solution σ_y is always the maximum principal stress at the tip of the plastic zone and experiments verify that Dugdale's second assumption (the plastic zone is a thin extension of the crack) is valid. However for an anisotropic material it is conceivable that σ_x might become greater than σ_y at the plastic zone tip depending on the value of the quantity $(\beta_1\beta_2 - \alpha_1\alpha_2)$ in equation (3.4); hence, σ_x could become the maximum principal stress. For such a case, the Dugdale model as normally defined is not applicable to an anisotropic material. The validity of a Dugdale type solution for an anisotropic

material thus depends on the condition $\sigma_y > \sigma_x$ which can be restated in terms of material properties using equations (3.4) and (3.5) as

$$\beta_1\beta_2 - \alpha_1\alpha_2 < \frac{Y}{Y-P} \tag{3.13}$$

where α_i and β_i are defined by equations (3.9) and (3.10), P is the external load, and Y is a constant stress which, as defined by Gonzalez, is related to the anisotropic yield properties of the material. If the inequality in equation (3.13) is not satisfied, a Dugdale type solution is no longer valid and it is thought that the material will tend to yield in some direction other than along the crack line. Condition (3.13) is illustrated graphically in Fig. 12 with the shaded region being the region where the Dugdale model is satisfied.

The principal difficulty in applying the preceeding analytical results to real materials is in finding real materials that are both anisotropic and homogeneous. Composite materials certainly provide the required anisotropy but they are inhomogeneous in general. Nielsen [36] indicates that uniaxial stretching of a polymer increases the elastic modulus in the direction of stretch and decreases it in the transverse direction. Since the preceeding analytical analysis can be specialized to the orthotropic case, it was anticipated that a homogeneous orthotropic material could be produced by means of uniaxial stretching of a polymer. Orthotropic refers to a body which possesses three orthogonal planes of elastic symmetry at each point in the body as opposed to an isotropic material whose properties do not vary with direction or orientation of the axes at that point.

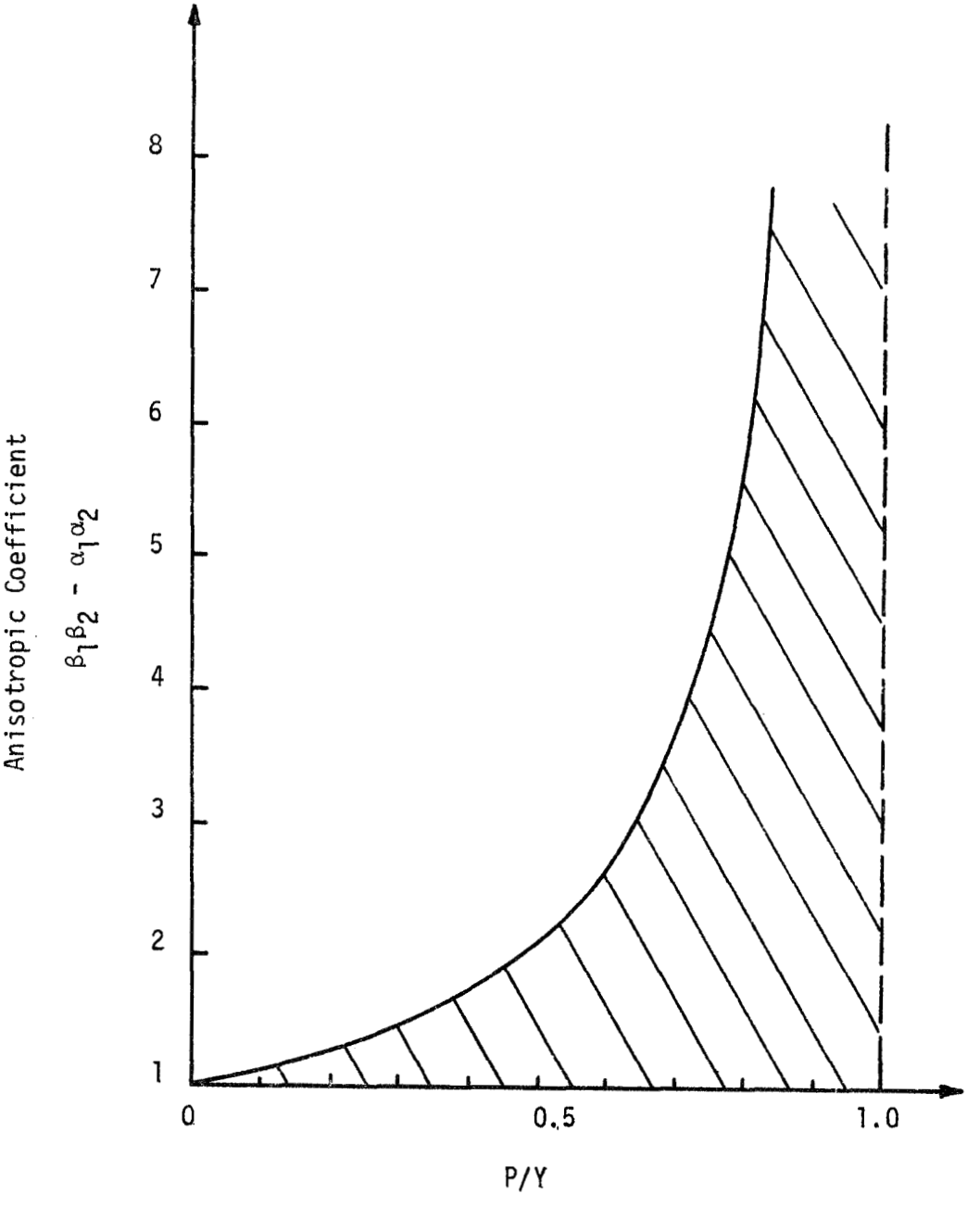

Fig. 12 Limit on Anisotropy for Anisotropic Dugdale Model.

In studying the ductile fracture of nonmetallic materials, polycarbonate appears to be a very suitable polymer for several reasons. It is a known ductile polymer and its stress-strain-optic properties are available in the literature [29], [37], [38], and [39]. It is highly birefringent thus lending itself to photoelastic analysis. Polycarbonate finds important technical application particularly in the aircraft industry where it is used as a glazing material for aircraft canopies, windows, windshields, etc. because of its strength to weight ratio. The stress-strain behavior is quite similar to that of mild steel and it is one of the few polymers that can be cold formed. For these reasons it is felt that polycarbonate holds some promise for use as a modeling material in attempting to analyze technologically important problems that arise concerning the behavior of steels and other metals.

The experimental effort can be divided into two general phases. The first portion concerns the production of an orthotropic material and the characterization of its elastic properties. The second part deals with a comparison of experimental results and the analytical theory presented by Gonzalez. As previously indicated the literature suggests uniaxial stretching as a means of achieving molecular orientation so as to produce an orthotropic material. Since polycarbonate is a known ductile polymer, it was anticipated that an orthotropic material could be manufactured by means of uniaxial stretching. Considerable effort was expended in attempting to produce the desired preorientation including stretching at elevated temperatures (temperatures in the neighborhood of the glass transition temperature), at room temperature, and cold rolling. The most successful technique appears to be cold rolling as it results

in a ratio of approximately 2:1 for the elastic moduli in the two principal directions. The actual procedure employed was to take an as received sheet of polycarbonate*, 0.020 inch nominal thickness, and make successive passes through a rolling mill until the thickness had been reduced by approximately one-half. A 50% reduction in thickness was found to be the maximum achievable before crazing occurred in the rolling process.

In order to describe the behavior of an orthotropic material in a plane stress situation it is necessary to determine five elastic constants: Young's moduli and Poisson's ratios in the two principal directions and the shear modulus (E_x, E_y, ν_x, ν_y, G_{xy}) together with information regarding the yield properties of the material. The next phase of the experimental program dealt with the characterization of the elastic properties of the orthotropic material produced by the rolling process.

Tensile specimens approximately 1 in. X 5 in. X 0.010 in. were cut from the rolled sheets using a template in conjunction with a high speed router. The tensile specimens were oriented parallel to the direction of rolling or perpendicular to it so as to permit determination of the elastic properties corresponding to the principal directions. Two sets of parallel lines approximately 0.900 inch apart were then lightly scribed on each specimen, one set being parallel to the direction of rolling and the other set perpendicular to it. The tensile tests

* Manufactured by the General Electric Corporation under the trade name Lexan.

were performed with the aid of an Instron Universal Testing Machine (Model TT-D-L, Instron Corporation, Canton, Massachusetts) operated at a constant elongation rate of 0.005 in./min. A series of photographs was taken at prescribed load increments for each tensile test to determine the elongation or contraction between the two sets of parallel lines on the specimen. The deformation was determined from the photographs using a Unitron Universal Measuring Microscope (Series TM, Unitron Instrument Company, Newton Highlands, Massachusetts). The microscope is equipped with a traveling stage to be used in conjunction with micrometer type screws that permit one to make linear measurements accurate to 0.0001 inch. The measured deformation was then converted to the corresponding strain value thus permitting determination of Young's moduli and Poisson's ratios for the principal directions. The shear modulus was determined by assuming the additional relation (see reference [35])

$$\frac{1}{G_{xy}} - \frac{2\nu_y}{E_y} = \frac{1}{E_y} + \frac{1}{E_x} \tag{3.14}$$

The yield properties of the material were also determined from the tensile tests described above. Yielding was presumed to occur at 0.4% offset strain. The equations of transformation (see reference [35]) were used to determine the elastic constants in situations where it was necessary to know the elastic properties at some angular orientation other than a principal direction. In such cases the yield properties were again established by means of tensile tests. Typical values for material properties determined from these tests were: E_x = 396,000 psi,

E_y = 244,000 psi, G_{xy} = 114,000 psi, ν_x = 0.43, ν_y = 0.26, yield strength in x-direction = 6200 psi, and yield strength in y-direction = 4200 psi.

In order to qualitatively verify some of the predictions of Gonzalez's solution, tensile specimens with a geometry similar to that shown in Fig. 13 were machined from cold rolled sheets of polycarbonate. The tensile specimens were prepared using a template in conjunction with a high speed router. A crack was simulated by machining a 0.180 in. X 0.020 in. slot in each specimen and each end of the slot was then notched with a razor blade. The notch measured approximately 0.015 in. in length and had a root radius estimated with the aid of a microscope to be no larger than 0.0002 in. Specimens were prepared with the line of the crack oriented at angles of 0°, 30°, 45°, and 90° with the direction of rolling (strong material principal direction) so as to observe the behavior of the material with a crack at various inclinations to the state of orthotropy. The tests were conducted on a Instron Universal Testing Machine operated at a constant elongation rate of 0.005 in./min. Photoelastic photographs were taken at various load levels throughout the tests.

The purposes of the fracture tests were twofold: (a) to observe if the crack proceeded in a direction other than along the original crack line depending on material orthotropy and (b) to measure the crack opening displacements at the center of the crack in order to provide a quantitative evaluation of the theory. The results of such tests are presented subsequently.

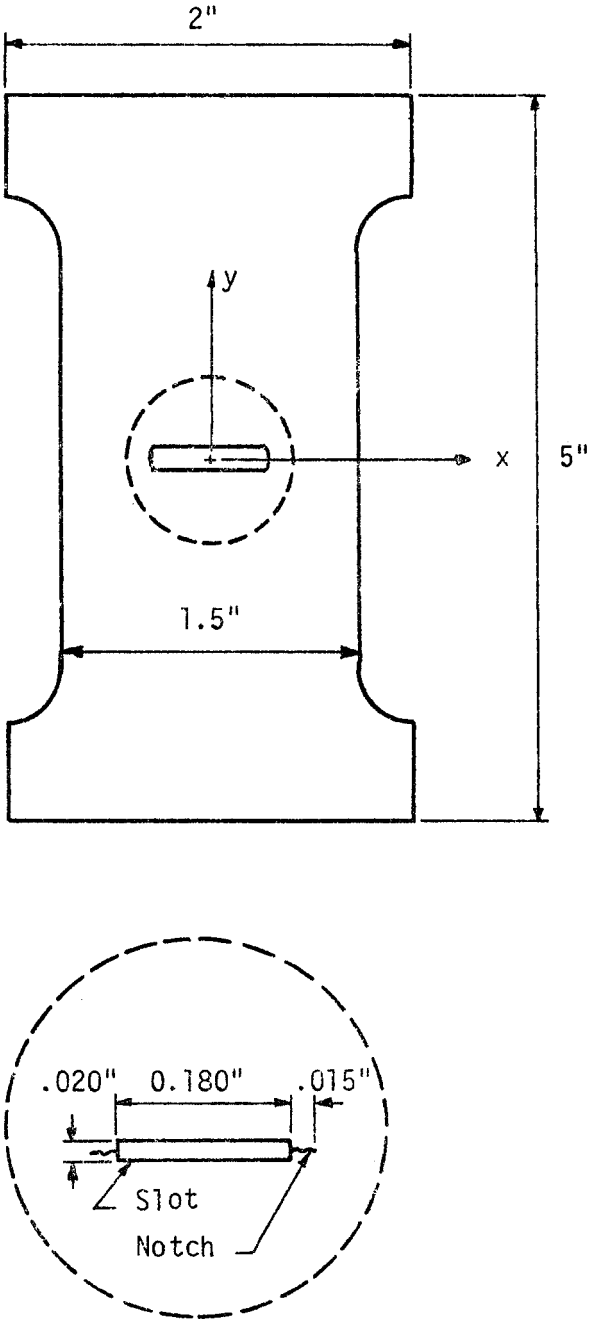

Fig. 13 Test Specimen Geometry

CHAPTER IV

RESULTS AND CONCLUSIONS

4.1 Analytical

In comparing the results of the modified problem presented in Chapter II to those obtained by Dugdale the following similarities are noted. The four assumptions listed early in Chapter II lead to the following equation for plastic zone size.

$$\frac{s}{a} = 2 \sin^2 \left(\frac{\pi}{4} \frac{P}{Y} \right) \tag{4.1}$$

In other words, the finiteness condition of Dugdale (equation (2.8)) remains unchanged only as long as the logarithmic singularity is retained in the stress functions. Since one of the purposes of the analytical problem was to investigate the influence of the assumed shear stress on the stress state in the vicinity of the crack tip, it was deemed important to retain this weak singularity.

The stress components σ_ρ and $\tau_{\rho\theta}$ on the elastic-plastic boundary obtained from the modified problem are the same as those predicted by Dugdale's solution. The effect of imposing a uniform shear stress on the plastic zone is to modify the stress component σ_θ on the elastic-plastic boundary as well as the displacements u and v at the surface of the crack and the elastic-plastic boundary. In both cases the stress and displacement components differ from Dugdale's results by an added term that is dependent upon the imposed shear stress. Typical

results of a comparison between Dugdale's results and the modified problem are presented in Figures 14 and 15. It is noted that the stresses differ only in the vicinity of the crack tip ($\theta = 0°$ in Fig. 14) and this is a consequence of retaining the weak logarithmic singularity in the stress functions. The displacements are not markedly different as evidenced in Fig. 15. It is thought that the small difference would be difficult to detect experimentally; furthermore, experimental verification would be compounded by the anticipated difficulty in measuring the shear stress that is presumed to exist along the plastic zone boundary.

At this point it would appear worthwhile to examine the results of the modified problem in terms of the justification cited in Chapter II. The principal motivation for the modification of the stress and displacement field associated with the Dugdale mathematical model was an attempt to realize a situation where the maximum stress and consequently the direction of plastic zone propagation would not coincide with the line of the crack. The solution to the modified problem does demonstrate the admissibility of stress states other than just uniaxial tension along the elastic-plastic boundary and this is in contrast to models adopted by other investigators. However, the maximum stress occurs at the crack tip and not at some adjacent point; thus, it is assumed that yielding would proceed along the crack line and not in some other direction. Of course there was no knowledge a priori that the proposed modification would lead to the desired result. In retrospect it would appear prudent to examine the nature of the analytical problem that was solved. The boundary value problem, mathematically speaking, consisted of a straight cut (the crack) loaded with normal and shearing

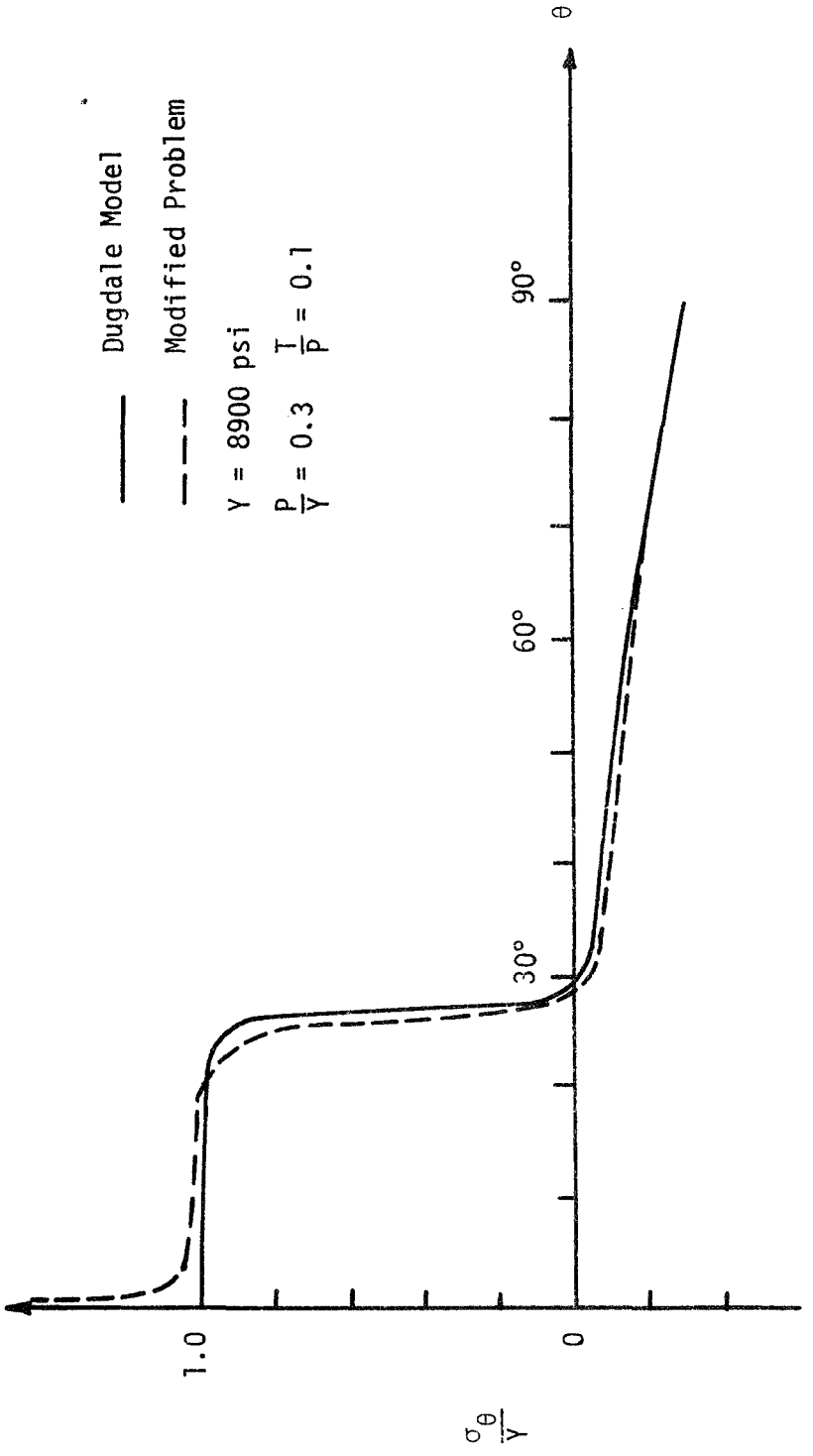

Fig. 14 Comparison of σ_θ Stress Component Between Dugdale Model and Modified Problem.

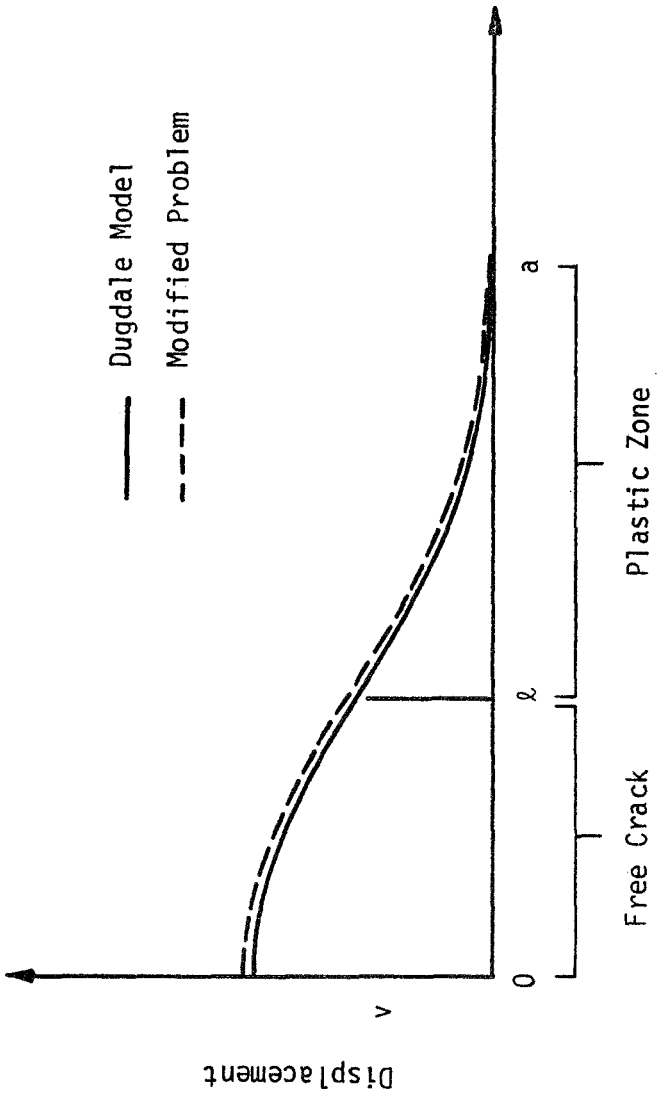

Fig. 15 Comparison of Crack Displacements Between Dugdale Model and Modified Problem.

forces. The results of this problem were used to calculate the stresses and displacements at the edge of the plastic zone boundary, and these calculations were based on the mathematical solution that was, strictly speaking, valid only for the problem of a straight cut. Of course in a real material the plastic zone boundary does not coincide with the crack. Perhaps a more physically realistic problem would be to consider a thin but finite ellipse with the presumed boundary loads rather than a straight cut. It would be possible to use the existing stress functions to calculate the nature of the stresses some small distance away from the crack line (where the plastic zone boundary has been observed in real materials [29]), but this problem is more formidable than the one solved in this investigation. This observation is made simply to point out the fact that if the stresses were calculated some distance away from the crack line, then a maximum stress state might occur at a point removed from the crack tip.

The physical motivation for assuming a constant shear stress along the plastic zone boundary was provided by Brinson's work [29] where it was observed that isochromatic fringes in the elastic region tended to turn and proceed parallel to the direction of the crack and plastic zone direction. Brinson also noted large deformations as well as large thickness changes occurring in the plastic zone. Perhaps it is not altogether surprising that plane linear elasticity does not completely provide an accurate description of the phenomena occurring at the crack tip in a ductile material.

4.2 Experimental

As previously mentioned, the experimental effort was directed toward a qualitative verification of the Dugdale model applied to an anisotropic plate as presented by Gonzalez [31], and for the experimental investigation the above results were specialized to the orthotropic case. One of the most interesting aspects of Gonzalez's solution was the application of the Mises yield criterion for a Dugdale type solution and the corresponding limits on the validity of the solution. There is perhaps some question as to the soundness of this approach. According to Foreman [40] the isotropic Dugdale model presupposes a Tresca yield criterion (yielding normal to the line of the crack). However Brinson [29] noted experimentally that the plastic zone is candle-flame shaped which might lead one to consider the Mises yield criterion as Gonzalez did for the anisotropic case. According to Gonzalez's results one might expect some sort of branching of the plastic zone to occur depending on material anisotropy. In other words the material might tend to deform in some direction other than along the original crack line. The goal of the experimental investigation was to verify if this is indeed the case. The fundamental question that this problem poses is: what is the correct form of the flow rule to employ for an anisotropic situation? It is hoped that the experimental results will lend some insight in seeking an answer to this question.

In comparing the experimental results of Gonzalez's solution one particular parameter of primary interest was the crack-opening displacement at the center of the crack. For an orthotropic material when

the axis of the crack is aligned with one of the principal material directions, the constants α_i and β_i defined by equations (3.9) and (3.10) reduce to the following

$$\alpha_1 = \alpha_2 = 0 \tag{4.2}$$

$$\beta_1 = \left(\frac{A - C}{B} \right)^{1/2} \tag{4.3}$$

$$\beta_2 = \left(\frac{A + C}{B} \right)^{1/2} \tag{4.4}$$

where

$$A = \frac{E_y}{2G_{xy}} - \nu_y \tag{4.5}$$

$$B = \frac{E_y}{E_x} = \frac{\nu_y}{\nu_x} \tag{4.6}$$

$$C = (A^2 - B)^{1/2} \tag{4.7}$$

At the center of the crack, the crack-opening displacement equation (see equation (3.12)) can be written as

$$\frac{E_y v}{Y\ell} = \frac{\beta_1 + \beta_2}{2\beta_1\beta_2} \frac{2}{\pi} \log \left[\frac{1 + \sin \theta_2}{1 - \sin \theta_2} \right] \tag{4.8}$$

where v is the displacement. The inequality of equation (3.13) that must be satisfied if the theory is applicable simplifies to

$$\beta_1\beta_2 < \frac{Y}{Y-P} \tag{4.9}$$

or

$$\beta_1\beta_2 = \sqrt{\frac{E_x}{E_y}} < \frac{Y}{Y-P} \qquad (4.10)$$

As seen from equation (4.10) if the crack is aligned with the weak material direction ($E_x < E_y$), the inequality will always be satisfied and the theory predicts that Dugdale behavior should be observed. This conclusion was supported by experiments on a specimen with the crack aligned in the weak material direction. As seen in Fig. 16A yielding is confined to the original crack line and no branching of the crack is observed.

On the other hand when the crack is aligned with the strong material direction ($E_x > E_y$) for small values of the external load P, the inequality of equation (4.10) will be violated and it is thought that branching of the crack might be possible. As the external load increases the inequality of equation (4.10) may or may not be satisfied depending on the ratio E_x/E_y. Typical results of experiments on specimens where the crack is aligned with the strong material direction are presented in Figures 16B and 17. In Fig. 17 equation (4.8) has been plotted and it is noted that the displacements predicted by the orthotropic theory are always less than those predicted by the isotropic theory. Experimental values for the crack opening displacements at the center of the crack were measured with the aid of a microscope from photographs taken during the fracture tests. These results are also plotted on Fig. 17 and the qualitative agreement between theory and experiment appears to be quite good. The values for the crack-opening displacements determined

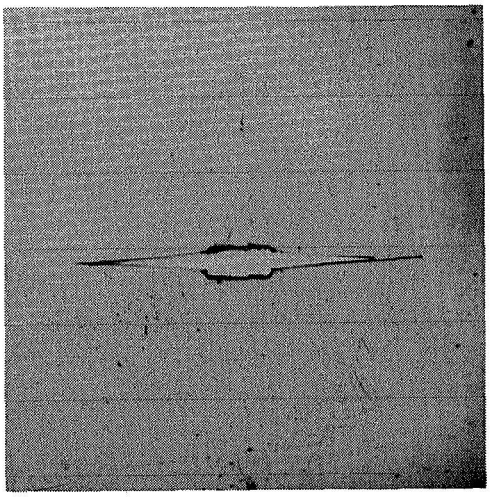

A. Specimen after loading when the axis of the crack was initially aligned with the weak material direction.

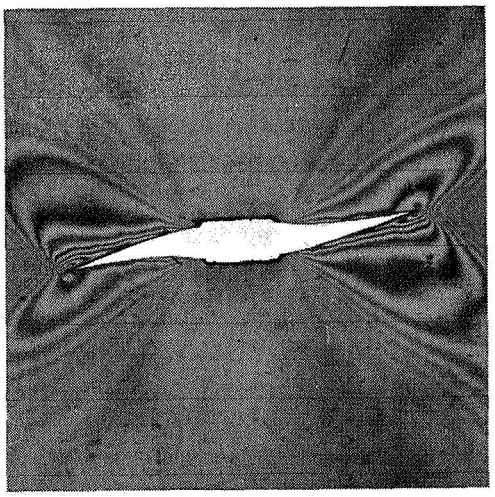

B. Specimen after loading when the axis of the crack was initially aligned with the strong material direction.

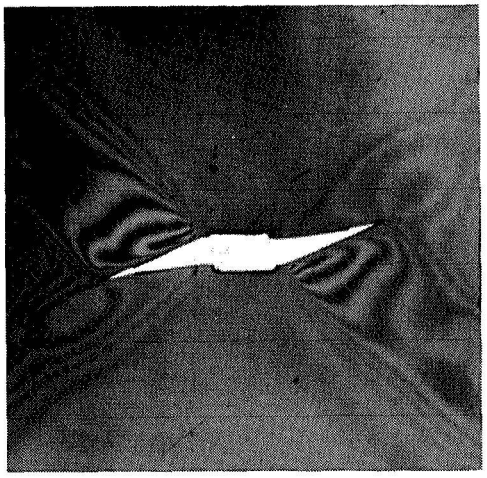

C. Specimen after loading when the axis of the crack was initially aligned at an angle of 30° with the strong material direction.

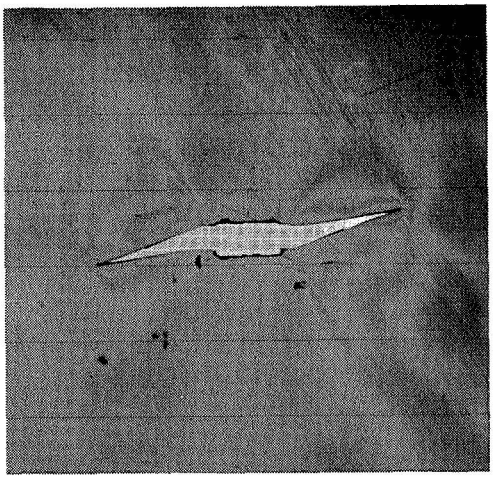

D. Specimen after loading when the axis of the crack was initially aligned at an angle of 45° with the strong material direction.

Fig. 16 Experimental Results.

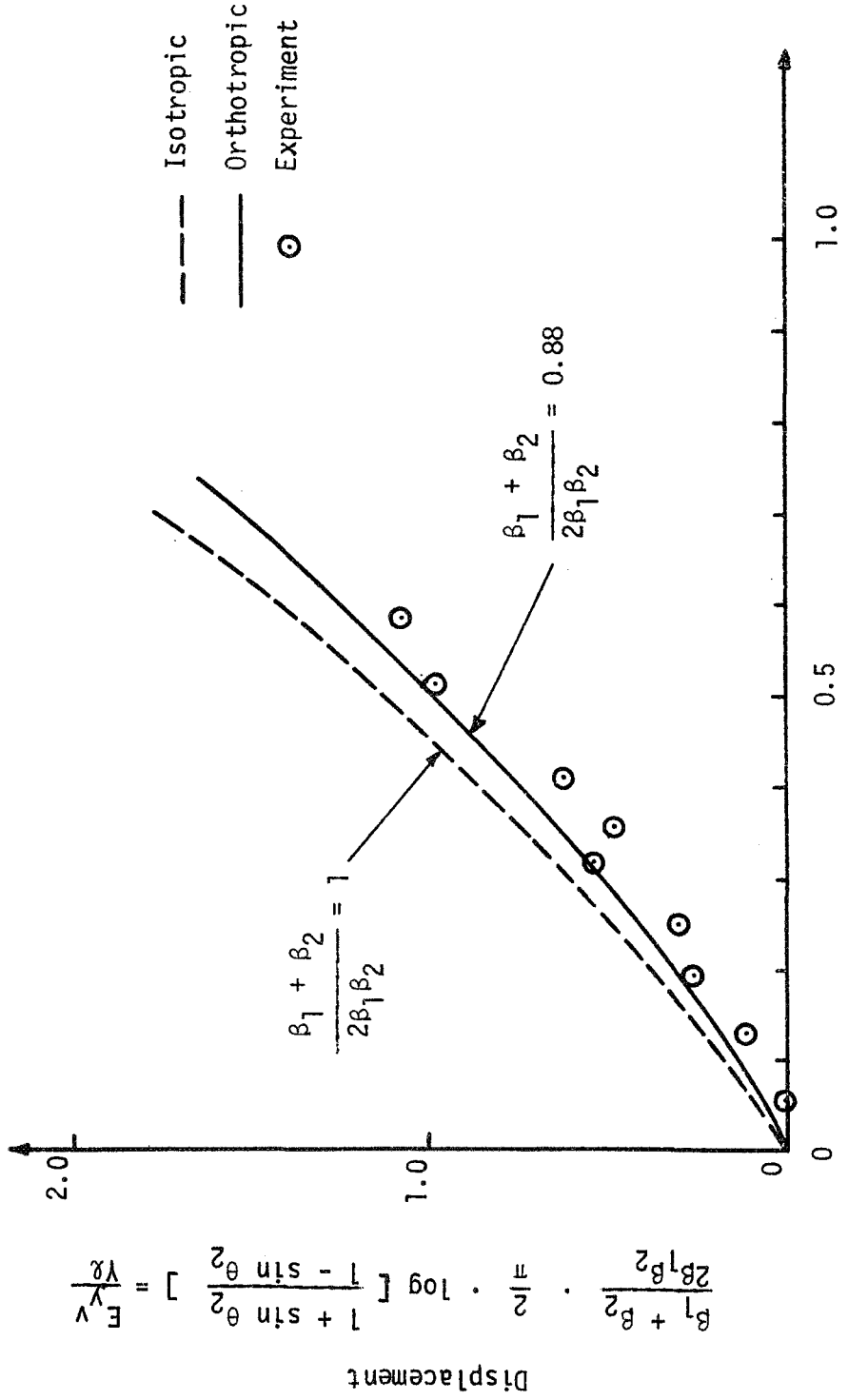

Fig. 17 Crack Opening Displacement at x = 0.

experimentally are consistently lower than those predicted by the analytical results and this leads one to conclude that the qualitative theoretical predictions are valid.

In order to study the behavior of the material when the axis of the crack was rotated with respect to the principal axes of orthotropy, fracture tests were conducted on specimens with the crack aligned at angles of 30° and 45° from the strong material direction. Typical results of these tests are shown in Figure 16C and 16D. It is noted that for both orientations the crack proceeded in a direction other than along the original crack line. It was observed in all cases when the crack was oriented in a direction other than coincident with the weak material axis that yielding occurred in a direction other than along the original crack line. Furthermore the crack extension always appeared to turn toward the weak material direction.

4.3 Conclusions and Recommendations

One interesting aspect of the analytical problem for future work would be to give additional consideration to the logarithmic singularity that arises from the assumption of a shear stress along the elastic-plastic boundary. If this term was annihilated in conjunction with the dominant singularity, the resulting finiteness condition would certainly differ from equation (2.8). Presumably, the resulting equation for the plastic zone size would also be altered as well as the expressions for stresses and displacements.

It is felt that the principal utility of the analytical work previously presented is in illustrating the possibility of more complex

stress states (other than uniaxial tension) existing along the elastic-plastic boundary in ductile materials containing cracks. While progress has been made in the understanding of contained plasticity, additional work needs to be done. If one is to accurately describe the local conditions present at the crack tip in a stressed body, it would appear that finite geometry changes should be considered. Also the three-dimensional character of "plane stress" yielding in plate problems is still not resolved. In polycarbonate for example, large thickness changes occur in the plastic zone, but this has not been incorporated in analytical models. Another area of interest is whether differing yield conditions or three-dimensional aspects are responsible for the Dugdale type plastic zone observed in some materials and the more diffuse flow patterns seen in others.

The present effort appears to qualitatively verify the anisotropic theory of ductile fracture presented by Gonzalez. A more detailed evaluation of the analytical model should entail a comparison of stresses but this is beyond the scope of this investigation. Additional consideration of such a theory may also help in understanding why various types of plastic zones develop in front of cracks in differing materials. Perhaps local anisotropy may be a means of identifying which type will occur in a given material.

One endeavor for future consideration suggested by the experimental program would be to investigate plastic zone sizes in anisotropic materials. As evidenced in Fig. 16 there is no well defined plastic zone occurring in any of the fracture tests. It is not clear whether anisotropy, the rolling process, or perhaps some combination of the two is responsible

for the lack of a well defined plastic zone.

It is felt that the analytical theory should have application in studying the fracture behavior of metallic crystalline materials, oriented polymeric materials, and composites. It is hoped that the present effort will assist in clarifying some of the problems associated with the ductile fracture of isotropic and anisotropic materials.

BIBLIOGRAPHY

1. Goodier, J. N., "Mathematical Theory of Equilibrium Cracks," Fracture: An Advanced Treatise, Volume 2: Mathematical Fundamentals, H. Liebowitz, (ed.). New York: Academic Press, 1968.

2. Cottrell, A. H., "Theoretical Aspects of Fracture," Fracture, B. L. Averbach, D. K. Felbeck, G. T. Hahn, and D. A. Thomas, (eds.). Massachusetts Institute of Technology: The Technology Press, 1959.

3. Wolock, I., Kies, J. A., and Newman, S. B., "Fracture Phenomena in Polymers," Fracture, B. L. Averbach, D. K. Felbeck, G. T. Hahn, and D. A. Thomas, (eds.). Massachusetts Institute of Technology: The Technology Press, 1959.

4. Paul, B., "Macroscopic Criteria for Plastic Flow and Brittle Fracture," Fracture: An Advanced Treatise, Volume 2: Mathematical Fundamentals, H. Liebowitz, (ed.). New York: Academic Press, 1968.

5. Erdogan, F., Crack Propagation Theories. NASA Contractor Report 901, October 1967.

6. Inglis, C. E., "Stresses in a Plate Due to the Pressence of Cracks and Sharp Corners," Transactions, Inst. Naval Architects, vol. 60, 1913.

7. Griffith, A. A., "The Phenomena of Rupture and Flow in Solids," Philosophical Transactions, Royal Soc. (London), Series A, vol. 221, 1920.

8. Sack, R. A., "Extension of Griffith's Theory of Rupture to Three Dimensions," Proceedings, Physical Society (London), vol. 58, part 6, 1946.

9. Sneedon, I. N., "The Distribution of Stress in the Neighborhood of a Crack in an Elastic Solid," Proceedings, Royal Soc. (London), Series A, vol. 187, 1946.

10. Irwin, G. R., "Fracture Dynamics," Fracturing of Metals, Am. Soc. Metals, Cleveland, 1948.

11. Orowan, E., "Energy Criteria of Fracture," Welding Research Supplement, vol. 20, 1955.

12. Irwin, G. R., "Onset of Fast Crack Propagation in High Strength Steel and Aluminum Alloys," NRL Report 4763, Proceedings, 1955 Sagamore Conference on Ordnance Materials, vol. II, Syracuse University Press, Syracuse, N. Y., 1956.

13. Irwin, G. R., "Analysis of Stresses and Strains near the End of a Crack," Journal of Applied Mechanics, vol. 24, 1957.

14. Sanders, J. L., "On the Griffith-Irwin Fracture Theory," Journal of Applied Mechanics, vol. 27, 1960.

15. Sih, G. C. and Liebowitz, H., "Mathematical Theories of Brittle Fracture," Fracture: An Advanced Treatise, Volume 2: Mathematical Fundamentals, H. Liebowitz, (ed.). New York: Academic Press, 1968.

16. Barenblatt, G. I., "Mathematical Theory of Equilibrium Cracks," Advances in Applied Mechanics, Vol. VII, New York: Academic Press, 1962.

17. Hutchinson, J. W., "Singular Behavior at the End of a Tensile Crack in a Hardening Material," J. Mech. Phys. Solids, vol. 16, 1968.

18. Hutchinson, J. W., "Plastic Stress and Strain Fields at a Crack Tip," J. Mech. Phys. Solids, vol. 16, 1968.

19. Rice, J. R. and Rosengren, G. F., "Plane Strain Deformation Near a Crack Tip in a Power-Law Hardening Material," J. Mech. Phys. Solids, vol. 16, 1968.

20. Dugdale, D. S., "Yielding of Steel Sheets Containing Slits," J. Mech. Phys. Solids, vol. 8, 1960.

21. Goodier, J. N. and Field, F. A., "Plastic Energy Dissipation in Crack Propagation," Fracture of Solids, D. C. Drucker and J. J. Gilman, (eds.). New York: Interscience, 1963.

22. _____, Fracture Toughness Testing and its Applications, ASTM STP 381, American Society for Testing and Materials, Philadelphia, 1968.

23. Berry, J. P., "Fracture in Glassy Polymers I," J. Poly. Sci., vol. 50, 1961

24. Berry, J. P., "Fracture Processes in Polymeric Materials II," J. Poly. Sci., vol. 50, 1961.

25. Broutman, L. J. and McGarry, F. J., "Fracture Surface Work Measurements on Glassy Polymers by a Cleavage Technique. I. Effects of Temperature," J. App. Poly. Sci., vol. 9, 1965.

26. Broutman, L. J. and McGarry, F. J., "Fracture Surface Work Measurements on Glassy Polymers by a Cleavage Technique. II. Effects of Crosslinking and Preorientation," J. App. Poly. Sci., vol. 9, 1965.

27. Lindsey, G. H., "Viscoelastic Fracture - An Expository Treatment of Polymer Failure," Technical Report NPS-57LI7111A, United States Naval Postgraduate School, Monterey, Calif., 1967.

28. Andrews, E. H., Fracture in Polymers, New York: American Elsevier Publishing Co., Inc., 1968.

29. Brinson, H. F., "The Ductile Fracture of Polycarbonate," Experimental Mechanics, vol. 10, February 1970.

30. Rosenfield, A. R., Dai, P. K., and Hahn, G. T., "Crack Extension and Propagation Under Plane Stress," Proceedings of the First International Conference on Fracture, T. Yokobori, T. Kawasaki, and J. L. Swedlow, (eds.), 1965.

31. Gonzalez, H., "A Study of Anisotropic and Viscoelastic Ductile Fracture," Ph.D. Thesis, Virginia Polytechnic Institute and State University, Blacksburg, Virginia, 1969.

32. Goodier, J. N. and Kannien, M. F., "Crack Propagation in a Continuum Model with Nonlinear Atomic Separation Laws," Technical Report No. 165, Division of Engineering Mechanics, Stanford University, 1966.

33. Muskhelishvili, N. I., Some Basic Problems of the Mathematical Theory of Elasticity, Groningen, The Netherlands: P. Noordhoff, 1963.

34. Savin, G. N., Stress Concentration Around Holes, New York: Pergamon Press, 1961.

35. Lekhnitskii, S. G., Theory of Elasticity of an Anisotropic Elastic Body, San Francisco: Holden-Day, Inc., 1963.

36. Nielsen, L. E., Mechanical Properties of Polymers, New York: Reinhold Publishing Corporation, 1962.

37. Gurtman, G. A., Jenkins, W. C., and Tung, T. K., "Characterization of a Birefringent Material for Use in Photoelasto-Plasticity," Douglas Report SM-47796, Missile and Space Systems Division, Douglas Aircraft Company, Inc., Santa Monica, California, January 1965.

38. Brill, W. A., "Basic Studies in Photoplasticity," Ph.D. Thesis, Stanford University, 1965.

39. Cloud, G. L., "Mechanical-Optical Properties of Polycarbonate Resin and Some Relations with Material Structure," Experimental Mechanics, vol. 9, November 1969.

40. Foreman, R. G., "Effect of Plastic Deformation on the Strain Energy Release Rate in a Centrally Notched Plate Subjected to Uniaxial Tension," J. Basic Engineering, vol. 88, March 1966.

AN INTERPRETATION OF INELASTIC BIREFRINGENCE

Mechanical and optical measurements and discussion of gross yielding of polycarbonate in uniaxial tension.

by H. F. Brinson*

Abstract

The relationship between plastic thickness change and plastic isochromatics occurring beyond the plastic tensile instability point of a uniaxial tensile specimen is investigated. Mechanical thickness change measurements and a hologram of thickness change are shown to be in close qualitative agreement with isochromatics in a region of gross plastic yielding. Analytical observations are discussed to aid the interpretation of the experimental results obtained. Finally, possible extensions and applications are discussed.

INTRODUCTION

For many years efforts have been made to extend the principles of photoelastic stress analysis to materials stressed beyond the elastic limit. In an early effort, Hetényi [1] investigated the photoplastic effect in a nylon copolymer and compared plastic slip band formation with theoretical results given by Nádai [2]. Several articles in reference [3] report on the basic optic laws of celluloid when stressed beyond the elastic limit, the use of birefringent coatings to investigate the plastic behavior of metals, and the use of creep properties to determine arbitrary stress-strain relations. The latter process has been extensively investigated by Hunter [4] using epoxy and polycarbonate materials. Frocht and Thomson [5] proposed a stress-optic law for celluloid which was then measured using the creep behavior of this material. Bayoumi and Frankl [6] proposed a general linear

---

* Associate Professor of Engineering Mechanics, Virginia Polytechnic Institute and State University

"equation of state" relating birefringence to a combination of stress and strain, and Fried and Shoup [7] proposed and measured a linear strain optic law for polyethelene.

More recently, a number of investigators have explored in depth the use of polycarbonate as a possible photoplastic material. Brill [8], Gurtman, et al. [9], and Whitfield [10] have performed experiments to characterize the optical and mechanical behavior of polycarbonate (lexan) and have applied the properties so found to the experimental solutions of elasto-plastic boundary value problems. Brinson [11] used the inelastic birefringence of polycarbonate to measure Dugdale type plastic zones in a uniaxial tensile strip containing an internal crack.

The study of photoplasticity involves several factors of which the more important ones are; material suitability, the basic stress-strain-optic laws of a material stressed beyond the elastic limit, mechanical and optical characterization, application to boundary value problems, and model to prototype transition. The first two factors seem to be the crux of successful photoplasticity. Inasmuch as many investigators have shown polycarbonate to be a suitable material, this investigation will explore certain aspects of the basic optic laws of polycarbonate when stressed beyond the elastic limit. Also, the material has been amply characterized by Brill, Gurtman and Whitfield [8,9,10] alleviating the need for further characterization for this investigation. Typical stress-strain-optic behavior of polycarbonate is displayed in Fig. 1. For more accurate and detailed information on behavior up to strains of 80% the reader is referred to the excellent work of Brill [8] from which the information in Fig. 1 was obtained.

In the efforts previously cited, photoplasticity has been studied mainly for usage as a problem solving tool. To this end <u>linear</u> stress or strain optic laws have been proposed, time dependent behavior has been used and in some cases efforts have been limited to regions near the yield point of a material, i.e. relatively small strains and linear stress or strain optic laws. As a result, much of the

earlier work could be explained on the basis of nonlinear elastic or viscoelastic material behavior. However material plasticity is definitely involved when materials exhibit slip band formation such as those found in references [1,8,9,10]. No information has been found which would aid a person in understanding the physical phenomenon represented by isochromatics in slip band or other regions of gross yielding. Earlier, the present author observed that isochromatic fringes in regions of gross yielding seem to be in qualitative agreement with lines of constant thickness. The present investigation was undertaken to verify these observations and thereby to provide new insight into the interpretation of isochromatics for polycarbonate in regions of gross plastic deformation.

EXPERIMENTAL PROCEDURES AND RESULTS

Uniaxial tensile tests were used as a method of obtaining and relating simultaneous thickness and birefringence measurements. Initial efforts were made to measure these variables during the progress of a uniaxial test, but it was found impractical to make in situ thickness measurements. As a result, uniaxial specimens were loaded and unloaded in such a way that permanent deformation, thickness change and isochromatics remained after unloading. This process had the added advantage that elastic properties would automatically be eliminated.

An isochromatic photograph of the residual fringes remaining after unloading of a 0.040" x 0.5" tensile specimen is shown in Fig. 2. To be more precise as to the formation of the yield zone shown, the specimen was loaded axially until the point of tensile plastic instability was reached. Loading was continued until the slip band shown in Fig. 2 was formed, after which the load was removed. As is readily understandable, various plastic deformation states remain in and around the slip band. If the point which undergoes the maximum deformation (thickness change) were traced along the stress-strain diagram of Fig. 1, it would reach approximately 20% strain and then unload elastically along the dashed line leaving a residual strain of approximately 15% and the isochromatic pattern indicated.

Thickness and Isochromatic Measurements

Thickness changes were measured utilizing a modified Taylor-Hobson surface roughness measuring device (Tally-Surf). The specimen was placed on a microscope stage with x-y travel capabilities and the Tally-Surf stylus was drawn across the nine longitudinal stations shown on the photograph of Fig. 2. Thickness variations were thus measured at each of twenty-five points on each station line. Accuracies of 1×10^{-4} in. were easily obtainable and it was also possible to insure that measurements taken represented actual thickness changes in the specimen. The results of these measurements for station lines 0.05 in., 0.20 in., and 0.40 in. are shown in Fig. 3.

Residual fringe orders were counted along each station line and these are also shown plotted in Fig. 3 for the same stations as the thickness measurements are indicated. Obviously, residual plastic thickness changes and residual plastic isochromatics have the same qualitative variation over the region of gross plastic yielding. Interestingly, where thickness change and fringe number are small, the two variables are nearly coincident, whereas when thickness change and fringe number are large, the two variables diverge considerably even though their trends are the same. These observations merely amplify the nonlinear nature of the relationship between thickness change and/or strain and birefringence for polycarbonate as is also indicated in Fig. 1.

Other differences between thickness change and birefringence are noted in Fig. 3 even when the variables are small. An obvious explanation results from consideration of initial local variation in the thickness of the material while in a stress-free state. Initial local variations of approximately 5×10^{-4} in. were certainly present and would not necessarily be represented by subsequent isochromatics produced by gross yielding. Thus, such local variations could easily produce significant differences in the results shown in Fig. 3.

Holographic Verification

While the qualitative relationship between plastic thickness variation and plastic isochromatics is clearly established as outlined in the foregoing comments, quantitative correlation was not possible. For this reason it was felt necessary to have additional qualitative data to reinforce the mechanical thickness measurements. In recent years holography has been shown to be an effective method of measuring and visaully observing thickness changes [12,13,14]. However, in the present case, a hologram of residual deformations of a permanently deformed specimen was desired, i.e., the specimen shown in Fig. 2. Also, the thickness changes involved represent larger variations than can be observed or recorded in conventional holography. For this reason, the same specimen as previously discussed and shown in Fig. 2 was immersed in an oil bath of nearly the same refractive index. A double exposure hologram of the oil bath with and without the specimen was taken. This procedure lowers the sensitivity of the process such that relatively large thickness changes can be ovserved [14].

The hologram obtained in the above manner is shown in Fig. 4. Comparison of Fig. 4 and Fig. 2 indicates again that isochromatics in a permanently yielded region and holographic interference fringes of permanent thickness changes in the same region are virtually identical. The reader is advised to note that the holographic interference fringes shown in Fig. 4 were taken without circularly polarized light and, as will be subsequently demonstrated, the fringes do not represent isochromatic fringes which can be obtained using holography [12,13,14].

A second specimen of polycarbonate was machined to be wedge shaped. Care was taken to insure that no residual isochromatic fringe pattern was induced by the machining process. A double exposure hologram of the oil tank with and without this stress free, isochromatic free, machined wedge is shown in Fig. 5. Obviously the interference fringes displayed in Fig. 5 represent thickness change and can

be used as a calibration of the holographic technique used. Using the calibration factor so obtained, thickness changes occurring in the specimen could be calculated from the hologram of Fig. 4. This was accomplished at one point and the result is plotted as point A in Fig. 3 and closely matches the previously recorded mechanical measurements.

ANALYTICAL OBSERVATIONS

In the foregoing it is apparent that a close qualitative correlation between plastic thickness changes and plastic isochromatics occur in a uniaxial speicmen of polycarbonate when stressed beyond the point of tensile instability. However, no reference has been made to the mechanism by which such behavior occurs nor has there been an attempt to analytically interpret these observations.

An anlytical model has been presented by Nadai [2] to explain slip band formation in metals, i.e., Lüders' lines. Hetenyi [1] used the same model to explain similar slip band formations in a nylon copolymer. This model can also be used in the present case.

Fig. 6 represents a schematic diagram of the uniaxial specimen and its predominate slip band which was previously shown in Fig. 2. Using elementary elastic analysis it is easily shown that,

$$\varepsilon_x' = \frac{1}{E}(\sigma_x' - \mu\sigma_y') = \frac{\sigma_o}{2E}[1 - \cos 2\alpha - \mu(1 + \cos 2\alpha)] \qquad (1)$$

Obviously, ε_x' varies between the two extremes $\varepsilon_x' = \varepsilon_y = \frac{\sigma_o}{E}$ and $\varepsilon_x' = \varepsilon_x = -\mu\frac{\sigma_o}{E}$. There exists an intermediate position such that $\varepsilon_x' = 0$ and if Poisson's ratio is taken up as $\mu = \frac{1}{2}$, this position will occur on a plane where $\alpha \simeq 35.3°$. Measurement of the orientation of the predominate slip plane in Fig. 2 yields an angle $\alpha \simeq 35.0°$. Thus, slip bands seem to occur on planes for which one component of the strain is zero. The explanation which has been given for this phenomena is

that yielding can take place on these planes without constraint from the surrounding medium [1,2].

While the above explanation may tend to explain the mechanics of slip band formation, it does not aid in the explanation of the accompanying optic effect of the marked increase of fringe order number in slip band regions. Quite obviously, from the earlier section on experimental results, thickness change in slip band regions seem to have a great deal of influence on the observed optic effect. In fact, these thickness changes require the existence of a three dimensional stress state in areas of gross yielding. However, using normal arguments of photoelastic theory, it is reasonable to infer that the stress normal to the plane of the specimen, σ_z, does not influence the optic effect. Also, it is apparent that the stress caused by permanent lateral contraction is nearly zero, $\sigma_x \simeq 0$. As a result, the stress state in a slip band can be thought of as uniaxial even beyond the yield point of the material. Therefore in the following, a uniaxial stress state will be assumed.

To aid further discussion idealized stress-strain-optic diagrams are shown in Fig. 7. A stress-optic law which would be consistent with photoelasticity and still be valid beyond the elastic limit would be,

$$\sigma = f_c^p \left(\frac{n_c}{d}\right) + \sigma_{y.p.} \left(1 - \frac{f_c^p}{f_c^e}\right) \tag{2}$$

where σ is the axial stress at a point, $\sigma_{y.p.}$ is the yield stress, n_c is the fringe order, d the thickness at the point in question, f_c^e the elastic material fringe value, and f_c^p the plastic material fringe value. Equation (2) is analogous to a strain hardening stress-strain law of the type,

$$\sigma = E^p \varepsilon + \sigma_{y.p.} \left(1 - \frac{E^p}{E^e}\right) \tag{3}$$

where ε is the strain at a point, E^e is an elastic modulus and E^p is a plastic modulus. The basic question to ask here is whether the idealized stress-strain-optic diagrams

shown in Fig. 7 are realistic representations of the behavior of polycarbonate. From consideration of Fig. 1 it is possible to infer that idealized stress-strain response is a close approximation to the behavior of polycarbonate. The only question is the magnitude of E^p. Here it is assumed that $E^p > 0$ but is small compared to E^e, i.e., $E^p << E^e$. In other words, while strain-hardening is assumed to take place, it is also assumed to be quite small. With these assumptions and with the aid of Fig. 1 it is possible to construct the idealized stress-optic response shown in Fig. 7 which would be quite similar to the idealized stress-strain response shown there also. Equation (2) is a logical consequence of this idealized response and can be rewritten as,

$$\left(\frac{n_c}{d}\right) = \frac{1}{f_c^p}\left(\sigma - \sigma_{y.p.}\right) - \frac{\sigma_{y.p.}}{f_c^e} \tag{4}$$

The interpretation of the stress-optic effect represented by equation (4) depends on whether the initial thickness, d_i, or the current thickness, d_c, at a material point is used. The proper choice is to use the current thickness as normal photoelastic theory dictates, even though in photoelasticity the initial thickness is most often used because there is little discrepancy between d_i and d_c in the elastic range. Use of both thicknesses are shown in Fig. 7 and it can be observed that a small decrease in thickness represents a relatively large increase in $\left(\frac{n_c}{d}\right)$ for the same stress level. In fact, it is intuitively obvious that should the thickness throughout the throat of a tensilve specimen remain uniform, then the fringe order would also be uniform. If the thickness varies over a slip band region, a multiple fringe pattern would be expected and fringes would then tend to be associated with lines of constant thickness. The earlier experimental evidence of Fig. 2 and Fig. 3 reinforce these remarks.

The residual fringe pattern of Fig. 2 after unloading can be predicted using equation (4) by assuming elastic unloading resulting in the equation,

$$\left(\frac{n_c^p}{d}\right) = (\sigma - \sigma_{y.p.})\left(\frac{1}{f_c^p} - \frac{1}{f_c^e}\right) \tag{5}$$

At this point it is also worth noting that uniaxial tension holographic interference fringes of thickness change for elastic deformation can be represented by the equation [12],

$$\sigma = \left(\frac{n_p}{d}\right) f_p^e \tag{6}$$

when n_p is the fringe order, d is the current thickness, and f_p^e is the isopachic material fringe value. While it is not known whether equation (6) can be extended to include inelastic deformations by rewriting in the form of (2), it is clear that holographic fringes and isochromatic fringes would have the same character in uniaxial tension. Therefore, it is not surprising that the hologram of Fig. 4 is similar to the isochromatic pattern of Fig. 2.

DISCUSSION

The experimental results of the present investigation indicates good qualitative correlation between lines of constant thickness change and isochromatic fringes in a slip band region of a uniaxial tensile specimen. The analytical observations presented also indicate that such a relationship should exist. The formulated stress-optic law has only been used as a means of explaining and discussing the relationship between thickness and isochromatic measurements. A strain-optic law could be used for the same purpose, particularly since thickness changes are related to the state of strain in a one- or two-dimensional stress state. However, due to the similarity between the stress-optic representation used herein and more rigorous elasto-plastic stress-strain equations, it would seem conceptually possible to formulate a theory of photoplasticity for three dimensions which would closely parallel the extensive theory of plasticity.

The holographic results may have possible future application in elastic and/or plastic stress analysis. As suggested by Hovanisian, et al [12], holographic

interferometry could be used in conjunction with two or three dimensional stress freezing, even for the relatively large deformations involved. This could be accomplished by using an oil bath of nearly the same refractive index to lower the sensitivity of the process.

References

1. Hetenyi, M., "A Study in Photoplasticity," Proc. First Natl. Cong., Appl. Mech., (1952).

2. Nadai, A., Theory of Flow and Fracture of Solids, Vol 1, McGraw-Hill, (1950).

3. Frocht, M.M., (ed.), Symposium on Photoelasticity, The MacMillan Company, (1963).

4. Hunter, A.R., "Development of a Photoelasto-plastic Method to Study Stress Distributions in the Vicinity of a Simulated Crack-Phase I and II," Lockheed Missiles and Space Company Report 4-05-65-11, (October 1965).

5. Frocht, M.M. and Thomson, R.A., "Studies in Photoplasticity," Proc. 3rd U.S. Natl. Cong., Appl. Mech., (1958).

6. Bayoumi, S.E.A. and Frankl, E.K., "Fundamental and Relations in Photoplasticity," Brit. Jour. of Appl. Phys., Vol. 4, (1953).

7. Fried and Shoup, N.H., "A Study in Photoplasticity: The Photoelastic Effect in the Region of Large Deformation in Polyethylene," Proc. 2nd U.S. Natl. Cong., Appl. Mech., (1954).

8. Brill, W.A., "Basic Studies in Photoplasticity," Ph.D. Thesis, Stanford University, (1965).

9. Gurtman, G.A., Jenkins, W.C., and Tung, T.K., "Characterization of a Birefringent Material for Use in Photoelasto-Plasticity," Douglas Report SM-47796, (January 1965).

10. Whitfield, J.K., "Characterization of Polycarbonate as a Photoelasto-Plastic Material," Ph.D. Thesis, VPI, (December 1969).

11. Brinson, H.F., "The Ductile Fracture of Polycarbonate," Experimental Mechanics, (February 1970).

12. Hovanesian, J.D., Brcic, V., and Powell, R.L., "A New Experimental Stress-Optic Method: Stress-Holo-Interferometry," Experimental Mechanics, (August 1968).

13. Fourney, M.E. and Mate, K.V., "Further Application of Holography to Photoelasticity," Experimental Mechanics, (May 1970).

14. Sampson, R.C., "Holographic Interferometry Applications in Experimental Mechanics," Paper No. 1567, Fall Meeting of SESA, (1969).

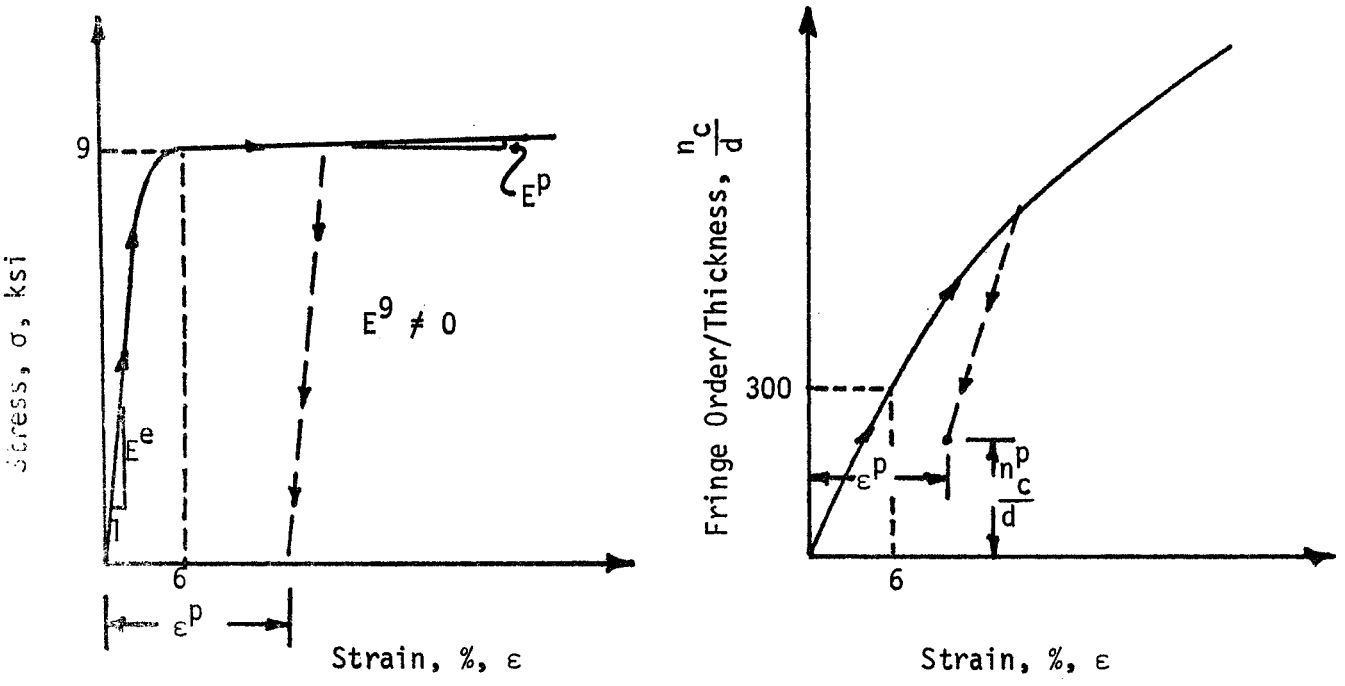

Fig. A1 Mechanical and Optical Behavior of Polycarbonate (From Brill [5]).

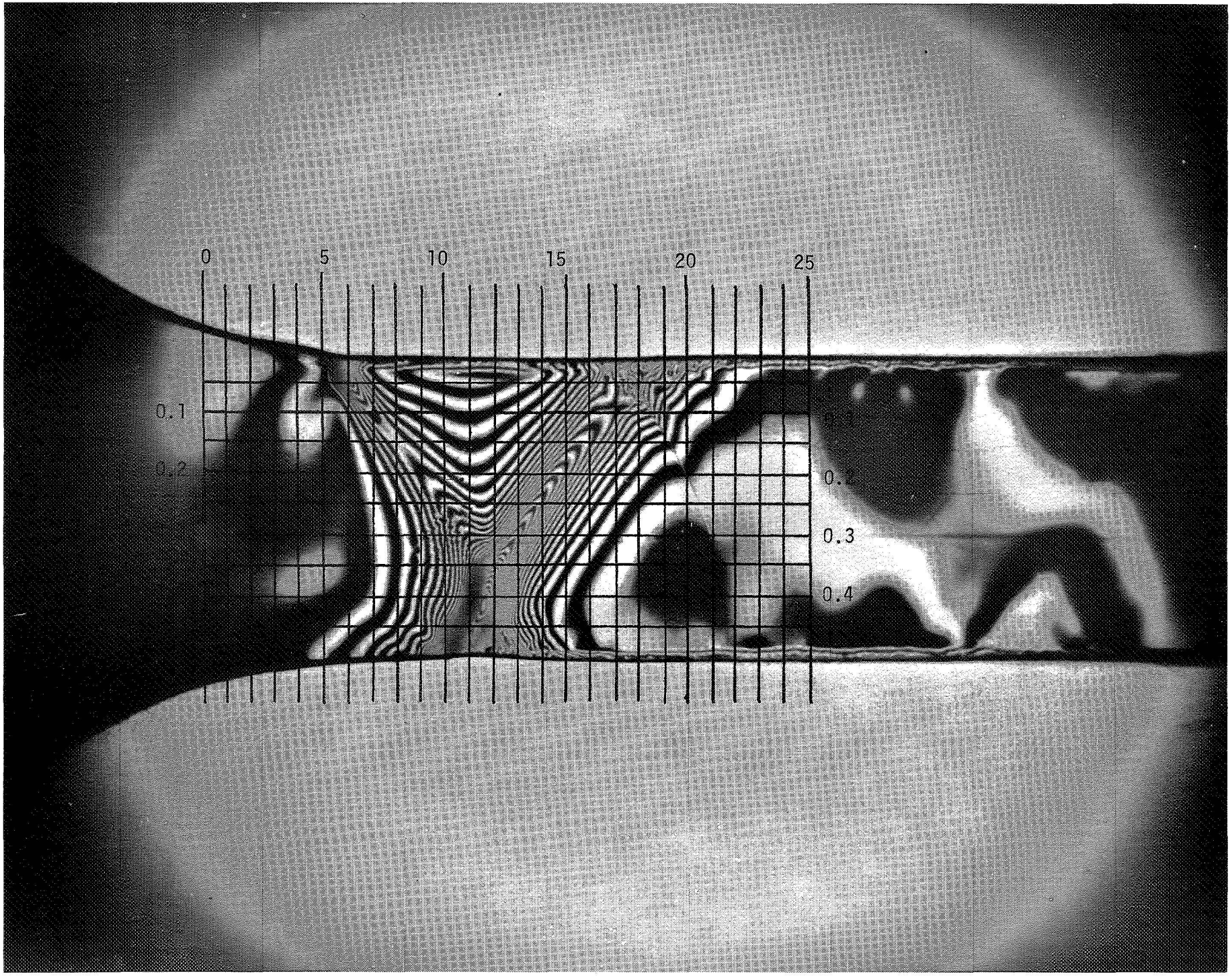

Fig. 2 Slip Band in Polycarbonate After Gross Yielding.

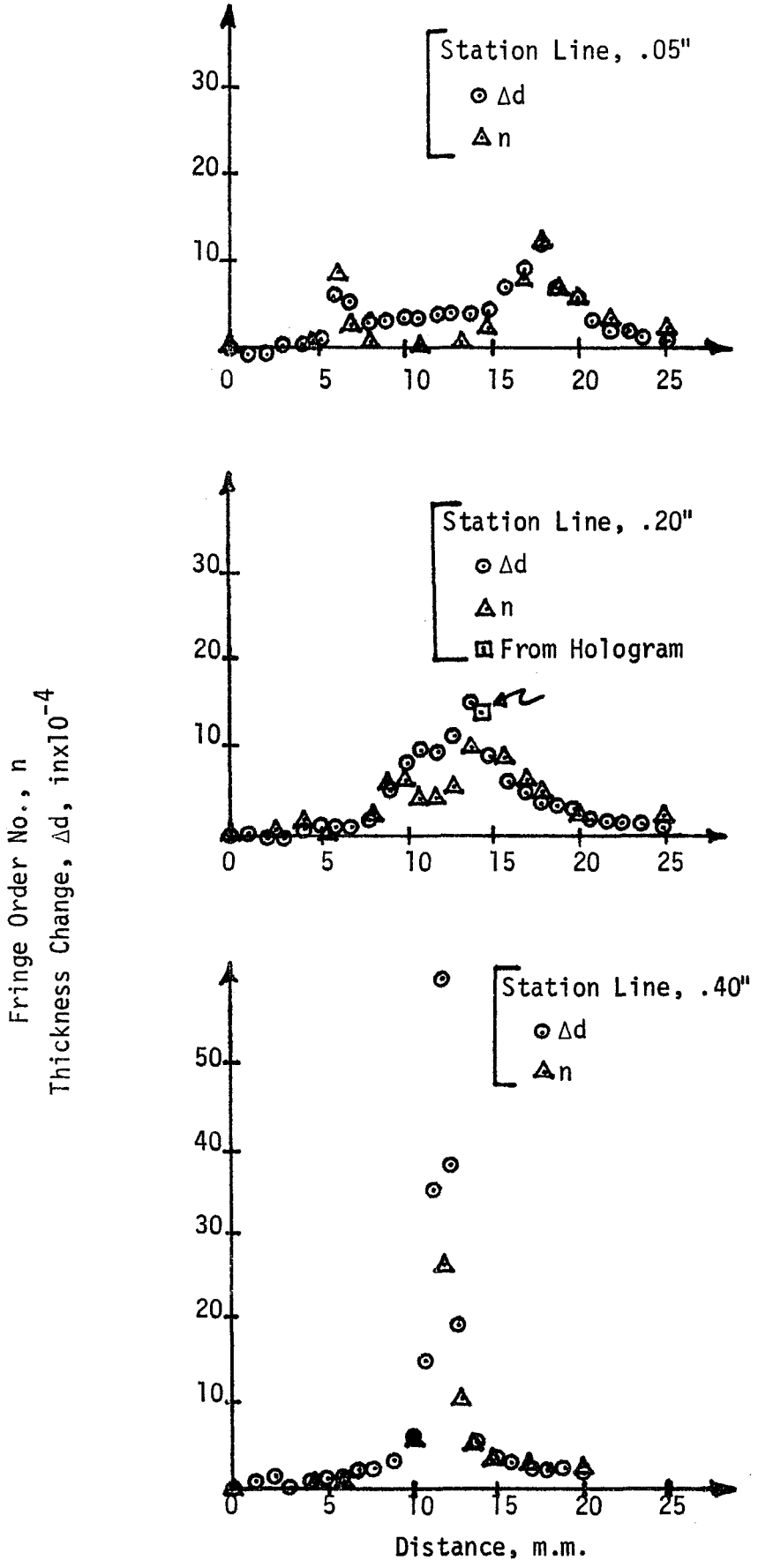

Fig. A3 Plastic Thickness Change and Isochromatics in the Slip Band of Fig. 2

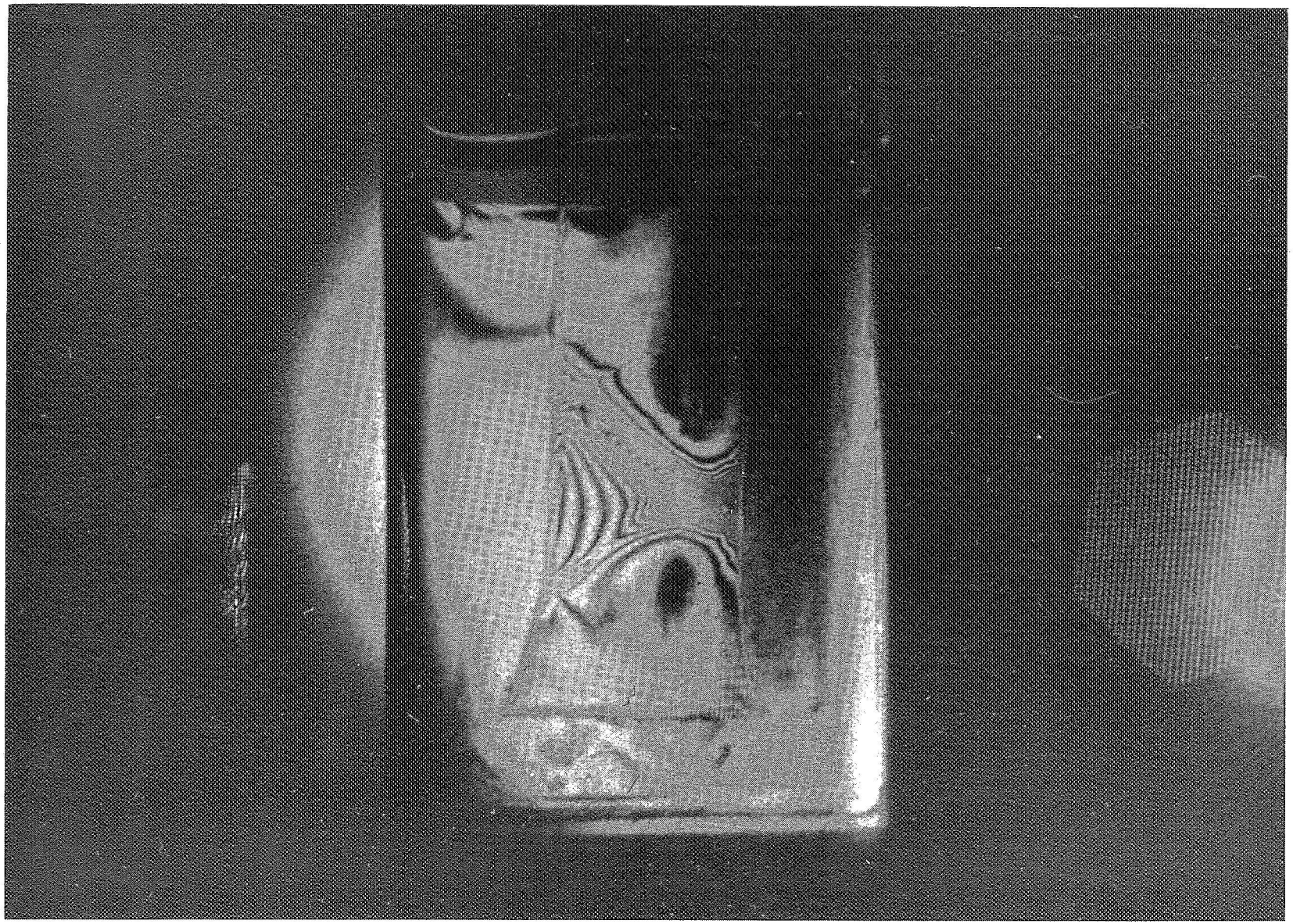

Fig. 4 Hologram of Slip Band Shown in Fig. 2.

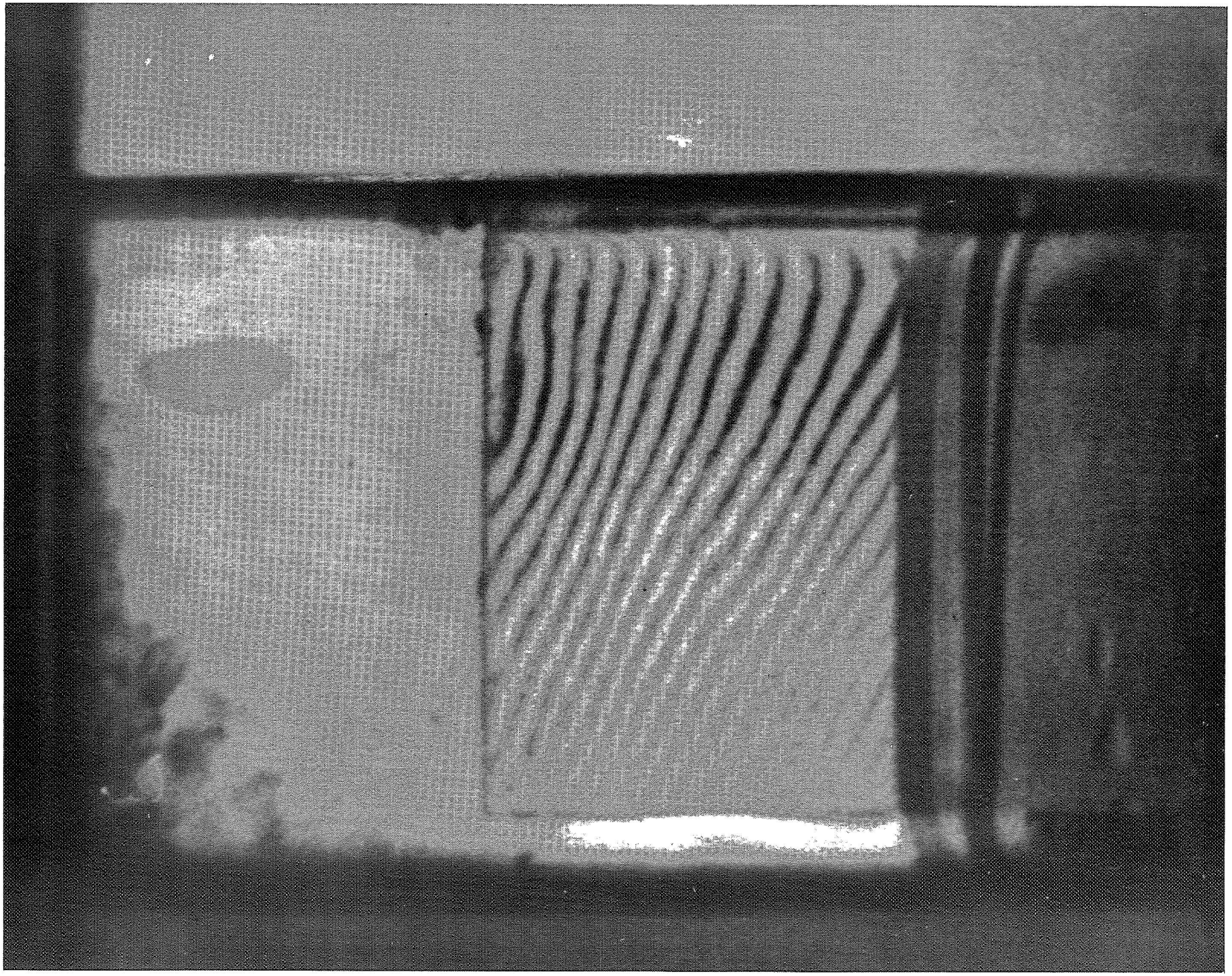

Fig. 5 Hologram of Calibration Wedge.

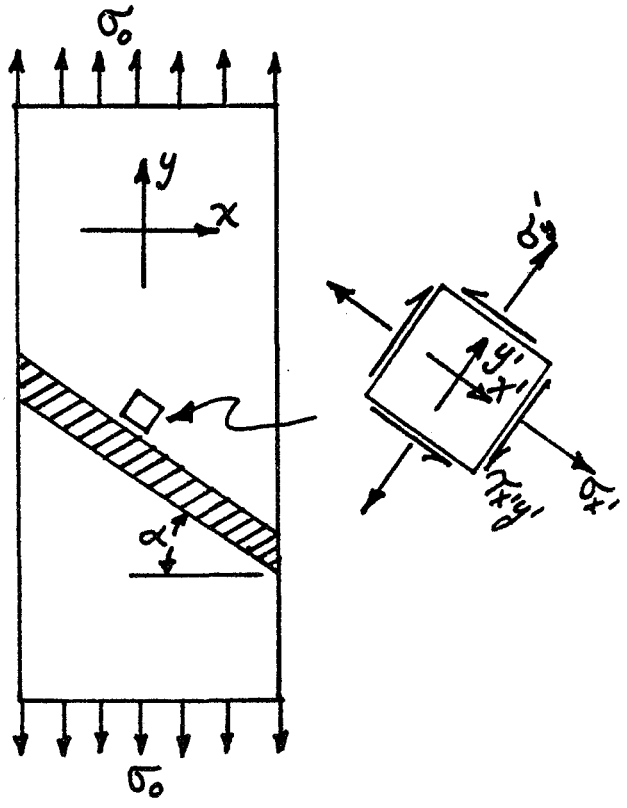

Fig. A6 Ideal Slip Band in a Thin Uniaxial Strip.

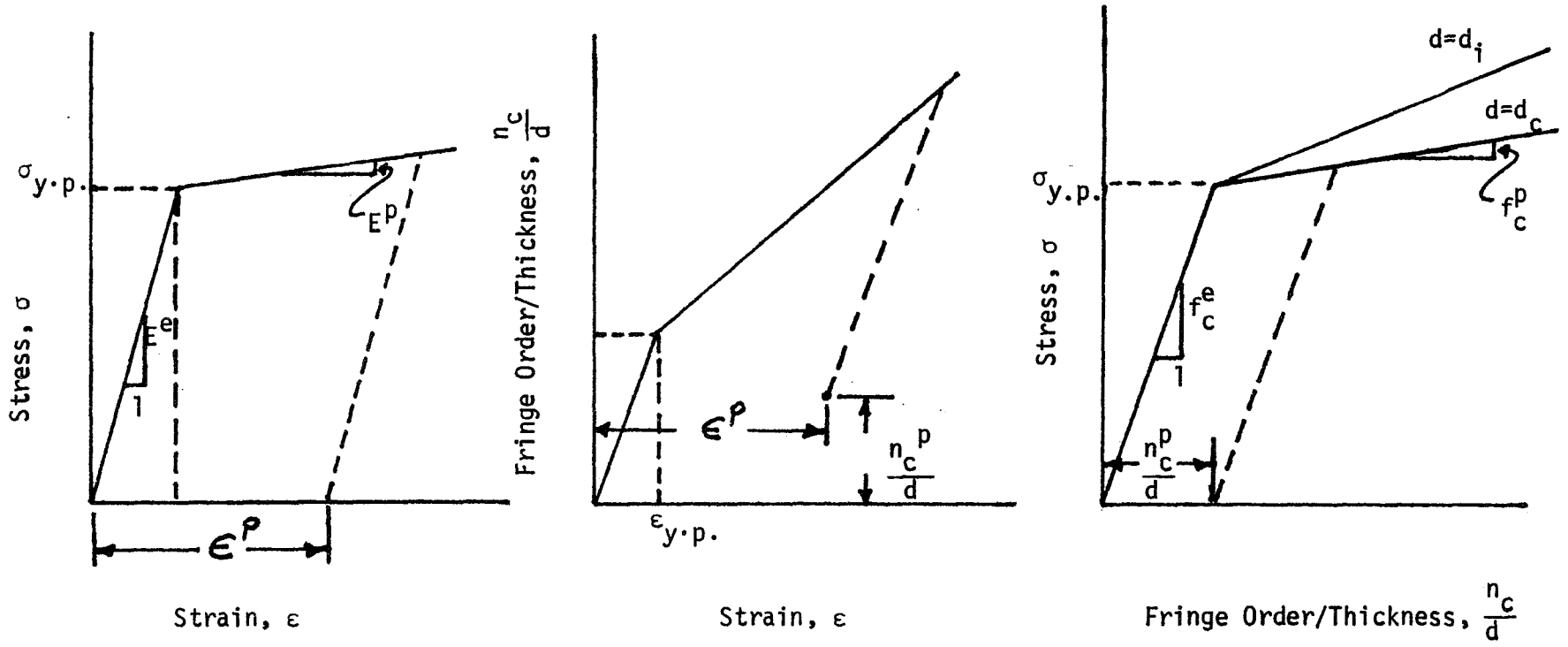

Fig. A7 Idealized Stress-Strain-Optic Behavior of Polycarbonate.